This is a repository copy of *Hunting For Eclipses: High Speed Observations of Cataclysmic Variables*.

White Rose Research Online URL for this paper:
http://eprints.whiterose.ac.uk/108581/

Version: Accepted Version

eprints@whiterose.ac.uk
https://eprints.whiterose.ac.uk/

Hunting For Eclipses: High Speed Observations of Cataclysmic Variables

L. K. Hardy,[1] M. J. McAllister,[1] V. S. Dhillon,[1,2] S. P. Littlefair,[1] M. C. P. Bours,[3,4]
E. Breedt,[4] T. Butterley,[5] A. Chakpor,[6] P. Irawati,[6] P. Kerry,[1] T. R. Marsh,[4]
S. G. Parsons,[1] C. D. J. Savoury,[1] R. W. Wilson[5] and P. A. Woudt[7]

[1] *Department of Physics and Astronomy, University of Sheffield, Sheffield, S3 7RH, UK*
[2] *Instituto de Astrofìsica de Canarias, E-38205 La Laguna, Tenerife, Spain*
[3] *Instituto de Fìsica y Astronomìa, Universidad de Valparaìso, Avenida Gran Bretaña 1111, Valparaìso, Chile*
[4] *Department of Physics, University of Warwick, Coventry CV4 7AL, UK*
[5] *Center for Advanced Instrumentation, Department of Physics, University of Durham, South Road, Durham, DH1 3LE, UK*
[6] *National Astronomical Research Institute of Thailand, 191 Siriphanich Building, Huay Kaew Road, Chiang Mai 50200, Thailand*
[7] *Department of Astronomy, University of Cape Town, Private Bag X3, Rondebosch 7701, South Africa*

ABSTRACT

We present new time-resolved photometry of 74 cataclysmic variables (CVs), 47 of which are eclipsing. 13 of these eclipsing systems are newly discovered. For all 47 eclipsing systems we show high cadence (1-20 seconds) light curves obtained with the high-speed cameras ULTRACAM and ULTRASPEC. We provide new or refined ephemerides, and supply mid-eclipse times for all observed eclipses. We assess the potential for light curve modelling of all 47 eclipsing systems to determine their system parameters, finding 20 systems which appear to be suitable for future study.

Systems of particular interest include V713 Cep, in which we observed a temporary switching-off of accretion; and ASASSN-14mv and CSS111019:233313-155744, which both have orbital periods well below the CV period minimum. The short orbital periods and light curve shapes suggests that they may be double degenerate (AM CVn) systems or CVs with evolved donor stars.

Key words: binaries: close - binaries: eclipsing - stars: dwarf novae, novae, cataclysmic variables.

1 INTRODUCTION

Cataclysmic variables (CVs) are binary systems in which a white dwarf accretes mass from a (usually) late-type, main sequence companion. The accretion tends to be via an accretion disk, or directly onto the poles of the white dwarf in the case of a strong magnetic field. In all cases, the donor star loses mass via Roche lobe overflow, and steady mass transfer is driven by a loss of angular momentum. For extensive reviews of CVs see Warner (1995) and Hellier (2001).

If the orientation of the orbital plane of a CV is coincident with our line of sight, eclipses may be observed. CVs often have complex eclipse structures, revealing different components of the system, including the accretion disk, the white dwarf and the bright spot, where the infalling material from the donor star encounters the disk. In certain systems these features are evident and clearly separated from one another, whilst in others they are not present, are very weak, or are blended together. In most CV systems there is the added stochastic variability component

known as flickering, which is due to random fluctuations in the accretion flow rate. Some systems show varying rates of accretion and disk radius, which can be observed as changes in the timing and depth of the bright spot eclipse.

When dwarf novae CVs display clear and separable white dwarf and bright spot eclipses, their light curves can be modelled allowing precise measurements to be made of the component masses and radii, in addition to other system parameters. In such cases, this information can be extracted without any form of spectroscopic study, e.g. Wood et al. (1986); Littlefair et al. (2008); Savoury et al. (2011); McAllister et al. (2016), and the validity of this method has been verified using time-resolved spectroscopy (Tulloch, Rodríguez-Gil & Dhillon 2009; Savoury et al. 2012; Copperwheat et al. 2012). Figure 1 shows an example of an ideal eclipse, with structure that is suitable for modelling.

Eclipsing CVs can therefore be useful in improving our understanding of CV evolution. Theoretical and empirical studies of the white dwarf mass distribution in CVs, and the properties of CV donor stars, both rely on the limited database of precisely measured CV system parameters.
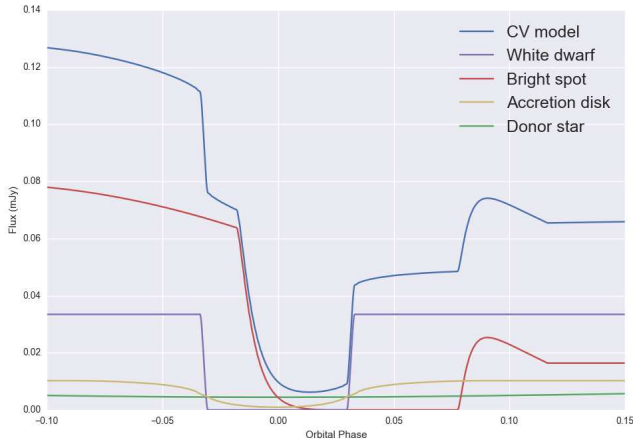
Figure 1. Artificial eclipse light curve, showing the different components of the model, which all contribute to the total light curve. An eclipse light curve showing clearly separated structure like this is ideal for modelling.

For example, the average white dwarf mass is considerably higher in CVs than in pre-CV systems and single white dwarfs. Explanations for this include rapid mass accretion during CV formation (Schenker & King 2002) or gradual mass growth via long-term stable accretion (Savoury et al. 2011), however Wijnen, Zorotovic & Schreiber (2015) ruled out both of these scenarios using binary population synthesis models. Recently this mass distribution discrepancy has instead been attributed to enhanced angular momentum loss in low-mass white dwarf CVs during early nova eruptions (Schreiber, Zorotovic & Wijnen 2016; Nelemans et al. 2016).

The study of CV evolution is also directly linked to the properties of the donor star, which can affect the rate of angular momentum loss in the system. Much work has gone in to producing a semi-empirical donor sequence which describes the mass, radius, effective temperature and spectral type of CV donor stars as a function of orbital period (Smith & Dhillon 1998; Patterson et al. 2005; Knigge 2006; Knigge, Baraffe & Patterson 2011).

However, these models of white dwarf and donor star evolution still require considerable refinement, since precise measurements of CV system parameters exist for fewer than 30 systems (Zorotovic, Schreiber & Gänsicke 2011). More measurements over a range of orbital periods are needed. Finding and characterising new eclipsing CVs will greatly help this process.

In this paper we present a search for new eclipsing CVs, predominantly in the northern hemisphere. Similar studies of CVs in the southern hemisphere have been conducted by Coppejans et al. (2014), Woudt et al. (2012), and in the preceding papers by that group. In addition, we also present a large collection of high speed observations of existing eclipsing systems, many of which already have published photometry, but of a lower time resolution. For all eclipsing systems we provide an evaluation of their suitability to be used in light curve modelling. These observations are part of an ongoing campaign to derive CV system parameters (McAllister et al. 2016 and references therein), and will form the observational basis of a future paper detailing the modelling of these systems.

2 CANDIDATE SELECTION

Dwarf novae routinely enter phases of brighter emission known as outbursts, due to thermal instabilities causing changes in viscosity of the accretion disk, dumping large amounts of material onto the white dwarf in a short period of time (Osaki 1996; Lasota 2001). New dwarf novae are being detected in outburst at a rate of at least one per day by current transient surveys. As of October 2016, the Catalina Real-Time Transient Survey (CRTS, Drake et al. 2009) had detected almost 1400 new CVs, the All-Sky Automated Survey for SuperNovae (ASAS-SN, Shappee et al. 2014) had found over 750, and the Mobile Astronomical System of TElescope-Robots (MASTER, Lipunov et al. 2010) had discovered almost 750. The Gaia astrometric surveying satellite is also now discovering transient events, including CVs, at a rate of several per day (Wyrzykowski et al. 2012; Blagorodnova et al. 2016). On top of these, many hundreds have been identified in the Sloan Digital Sky Survey (SDSS, Gänsicke et al. 2009; Szkody et al. 2011) and by a vast network of amateur astronomers. See for example *vsnet* (Kato et al. 2004) and the Center for Backyard Astrophysics (Patterson et al. 2013).

Our aim was to find new eclipsing systems amongst the CVs found in these surveys. Starting in 2014 with a list of nearly 2000, we first rejected those systems which were not visible or too faint in quiescence to be studied with our main facility in La Palma (see Section 3). We also rejected any systems which had already been studied at sufficiently high time resolution to rule out eclipses. These include systems which have already been studied with time-resolved photometry (e.g. Coppejans et al. 2014), and systems which have been closely followed by amateur observers. For example, *vsnet* have studied many systems whilst in outburst in search of superhumps[1] sometimes at high enough cadence to determine an orbital period and rule out eclipses.

At the end of this process we were left with around 80 systems eligible for follow up, and this number has grown gradually since our observing campaign began. We began by observing the brighter targets, and those which were already suspected to be eclipsing according to other studies. This could be either from spectroscopy suggesting that the accretion disk is close to edge-on (e.g. Breedt et al. 2014), or from long-term light curves provided by CRTS, for example, that show regular dips or faint measurements which are often due to eclipses.

3 OBSERVATIONS

For newly discovered CVs, initial observations were made with *pt5m*, a 0.5m telescope located at the Roque de

---

[1] Superhumps are hump-like variations in the light curve of outbursting dwarf novae, due to a projection effect seen when the tidal torques of the secondary star entice the heated accretion disk into an elliptical geometry (Whitehurst 1988; Hellier 2001).

los Muchachos Observatory on La Palma (Hardy et al. 2015). The telescope is robotic and sits on the roof of the control-room building of the 4.2m William Herschel Telescope (WHT). We aimed to obtain light curves of new CVs spanning upwards of 5 hours, with cadences of 1-2 minutes, as this should be sufficient to discover eclipses in most systems (see Section 5).

If eclipses were seen and a period could be measured, we then observed the systems at high time-resolution (few seconds) using either ULTRACAM on the WHT (Dhillon et al. 2007) or ULTRASPEC on the 2.4m Thai National Telescope (TNT, Dhillon et al. 2014). Both are imagers utilising frame-transfer CCDs for high cadence, low dead-time (of order 10ms) observations. ULTRASPEC has a single channel, whilst ULTRACAM has three channels, and can therefore observe in three filters (e.g. u', g', r') simultaneously.

In Section 6 we also present new observations of CVs which were already known to be eclipsing. Along with the WHT and the TNT, some of these observations were conducted at other telescopes, such as the 3.6m New Technology Telescope (NTT) at La Silla or the 8.2m Very Large Telescope (VLT) at Paranal, both in Chile. A select few systems were also observed with the 9.2m South Africa Large Telescope (SALT) and its SALTICAM instrument (O'Donoghue et al 2006). A log of all observations is presented in Table B1, an extract of which is presented here. The full version is available online.

In all observations, we performed differential photometry using bright stars near to the target as comparison stars. The fluxes of the target and comparison stars were extracted using variable aperture photometry with the ULTRACAM pipeline reduction software (Dhillon et al. 2007). For particularly faint targets, the optimal photometric extraction technique of Naylor (1998) was used. We calculated the magnitudes of the comparison stars by extracting their full flux using large, fixed apertures, then flux calibrated these using measured extinction coefficients and instrumental zeropoints. The flux of the target was then calibrated using the calculated magnitude of the comparison star.

We supply average out-of-eclipse magnitudes in Table B1 primarily as a guide to show when systems are in outburst, or to demonstrate which systems show strong variability. However, since the zeropoints measurements (based on observations of photometric standard stars) are made less frequently than the science observations, these magnitudes should always be considered estimates. Systematic uncertainties of 0.2 magnitudes or more could be introduced by variable extinction or high altitude clouds. The atmosphere tends to be stable and clear in La Palma and in Chile, but in Thailand there is frequently low altitude haze, as well as thin, high altitude clouds, which strongly affect the extinction coefficients and zeropoints. Therefore all measured magnitudes from the TNT are to be treated with extra caution.

Most observations made with ULTRASPEC at the TNT were conducted in the standard SDSS filters, but sometimes we used a non-standard $KG5$ filter. This filter encompasses the SDSS u', g' and r' pass bands, and can therefore obtain better signal-to-noise ratios on fainter targets than individual SDSS filters. The obvious disadvantage here is that it is not easy to convert the measured counts into a calibrated flux. We describe our solution to this problem in Appendix A.

4 RESULTS: NEW ECLIPSING SYSTEMS

We present 13 CV systems which were either unknown to be eclipsing, were suspected eclipsers, or whose eclipsing nature has only recently been published. Most discoveries were made with $pt5m$ observations over several nights, in the Johnson V filter. When eclipses were found, mid-eclipse times were measured by fitting a Gaussian to the eclipse profile, this being the simplest and fastest method. The quoted uncertainties in these mid-eclipse times are the statistical errors given by the Gaussian fit. We expect the true uncertainty to be up to an order of magnitude larger and dominated by the systematic error inherent in treating these complex eclipse shapes as Gaussians.

Ephemerides were obtained by a linear fit to the eclipse times. When fitting for an ephemeris, we always selected the orbital cycle zero-point (T_0) which minimised the covariance between P and T_0. Occasionally we omitted some mid-eclipse times from the ephemeris fit, if for example the system was in outburst, there were orbital cycle ambiguities, or the times had very large errors (often the case with $pt5m$ observations). We conducted additional checks on period measurements using phase-dispersion-minimisation (PDM, Stellingwerf 1978) of all the available, normalised light curve data. The resulting PDM periodogram shows troughs at potential orbital periods, and visual inspection of the light curves phase-folded on these potential periods was sufficient to confirm or reject reliable periods. In all cases we had sufficient eclipse and out-of-eclipse data to eliminate period aliases. The derived ephemerides of all systems are presented in Table 3.

Once a reliable period had been derived, we then attempted to investigate the eclipse structure by observing the system at high time resolution. Details of these observations are included in Table B1. In high cadence observations, the Gaussian fit to an eclipse profile is unsuitable, because the different components of the system are clearly visible. In this case, we use the mid-point of the white dwarf eclipse as the mid-eclipse time, determined from measurement of white dwarf mid-ingress and mid-egress. We supply the mid-eclipse times in Table B1 in case this information is useful to future orbital period variability studies (e.g. Parsons et al. 2010; Bours et al. 2016), but remind the reader that eclipse times measured by $pt5m$ suffer from the systematic uncertainty introduced by treating the eclipses as Gaussians.

High-speed eclipse light curves for each new object are shown in Figure 2. We briefly discuss each system below, and comment on the light curve morphology. Our judgement on the suitability for light curve modelling of each object is included in Table 3.

ASASSN-13cx: Discovered by ASAS-SN[2] with an outburst to $V = 15.5$ magnitudes, from $V = 18$ as

---

[2] References for ASAS-SN transients are not always available. See the ASAS-SN webpage at http://www.astronomy.ohio-state.edu/~assassin/transients.html

Table 1. Journal of Observations. Some object names have been shortened. Start(MJD) is the start time of each observing run, given in MJD(UTC). Mid-eclipse times are given in BMJD(TDB) and the number in parentheses is the uncertainty in the last digit. Note that *pt5m* mid-eclipses times are estimated using a Gaussian fit and will suffer from additional systematic uncertainty. T_{exp} is the exposure time in seconds and is supplied as $T_{blue}/T_{green}/T_{red}$ for the three beams of ULTRACAM. ΔT is the duration of the observing run in minutes. Mag. is the estimated out-of-eclipse magnitude. This is an extract showing only one object. The full table containing all 74 objects is available online.

Object	Start (MJD)	Mid-eclipse time (BMJD)	T_{exp} (s)	ΔT (min)	Tel./Inst.	Filter	Mag.
1RXS J180834.7+101041	55316.33464	55316.3613(3) 55316.4310(3)	6/2/2	141	NTT/UCAM	$u'/g'/r'$	16.9/16.9/16.6
	55334.37156	55334.4299(3)	10/2/2	101	NTT/UCAM	$u'/g'/r'$	17.0/17.0/16.8

recorded in the NOMAD catalogue (Zacharias et al. 2004). ASASSN-13cx also showed previous outbursts in the Catalina Sky Survey (CSS, part of CRTS), as well as fainter measurements indicating eclipses. During an outburst in 2014, *vsnet* observers were able to confirm the eclipsing nature and estimate a period (Kato et al. 2015). The high-speed eclipse structure shows clearly separated egress for the white dwarf and bright spot. The ingress of the bright spot is less clear.

ASASSN-15au: Discovered by ASAS-SN during an outburst to $V = 15.3$ magnitudes, from a quiescent SDSS magnitude of $g = 17.8$. It also shows variability of up to 3 magnitudes in archival CSS and Mount Lemmon Survey (MLS, part of CRTS) light curves, including outburst and eclipse-like faint measurements. We found multiple eclipses in *pt5m* light curves, and conducted high speed observations with ULTRASPEC. These observations show weak features that may be the bright spot ingress and egress, but further study is required.

ASASSN-15bu: Shows previous outbursts in the CSS light curve, as well as multiple dips signalling eclipses. *vsnet* (alert 18228) folded the CSS data to find a coherent orbital period of 110 minutes. We confirmed the eclipsing nature with 4 ULTRASPEC observations. No clear bright spot features are visible in the light curve, but a higher signal-to-noise light curve is needed to be certain that no features exist.

CSS110113:043112-031452: Discovered via a super-outburst in CRTS[3], from a quiescent magnitude of $V = 19$-20 to $V = 15$. The *vsnet* collaboration discovered eclipse signals and estimated an orbital period of 1.58 hours (alerts 12614, 12661), but no detailed studies have yet been published. We confirmed the eclipsing nature with observations of 12 eclipses in varying conditions. Sometimes the bright spot signal is hidden in noisy data or blended with the white dwarf, but throughout 2012 the ingress and egress are clearly separable. In this system it appears that the white dwarf begins exiting eclipse before the bright spot has finished entering eclipse.

CSS111003:054558+022106: Initially discovered as a planetary nebula and also known as Te 11 (Jacoby et al. 2010). It was shown to be eclipsing, with an orbital period of 0.12 days, before its reclassification as a CV (Miszalski et al.

___
[3] References are often not available for CRTS discoveries, though all transients are available online at `http://crts.caltech.edu/` and the discovery of CVs in particular is discussed in Drake et al. (2014).

2011). Drake et al. (2014) took spectra of the object, which showed very strong double-peaked Balmer emission lines, as well as [OIII] emission presumably associated with the nebula. Recently, Miszalski et al. (2016) presented a detailed study of the eclipses, using high cadence observations to extract its approximate system parameters using the light curve modelling technique. They also proposed that the nebula surrounding the system may in fact be the remnants of a nova eruption 1500 years ago. Despite being a faint source, a few of our eclipses showed well-separated bright spot and white dwarf features.

CSS111101:233003+303301: Discovered via an outburst of around 2 magnitudes from the quiescent level observed in SDSS (g=18.9-19.5). The system shows numerous faint dips in its CSS light curve, leading CRTS to suspect this system might be eclipsing. We confirmed the presence of eclipses and conducted high speed observations with ULTRASPEC. The light curve is dominated by strong flickering, and the eclipse is shallow, suggesting a possible grazing eclipse.

CSS131106:052412+004148: Has a quiescent magnitude in SDSS of $g' = 18.3$. The CSS light curve shows multiple outbursts in recent years, as well as occasional faint measurements, prompting us to search for and subsequently discover eclipses with *pt5m*. The high-speed eclipses show separation between the white dwarf egress and bright spot egress, although separation of the ingresses is less clear.

MASTER OT J003059.39+301634.3: Discovered by MASTER (Shurpakov et al. 2014a) with an outburst to 16.1 magnitudes (unfiltered). It is listed as $g = 18.1$ in SDSS (Ahn et al. 2012), though we suspect this magnitude may have been observed during a brightened state, as the USNO-B1.0 catalogue (Monet et al. 2003) and our own observations suggest it is fainter than 19th magnitude in B and V. We discovered eclipses and obtained several high cadence light curves, which display a clear white dwarf eclipse. There is also a suspected bright spot component, but one which eclipses slowly and follows directly after the white dwarf eclipse. It is also unclear exactly where the transition from bright spot egress to full out-of-eclipse flux occurs due to flickering.

MASTER OT J192328.22+612413.5: Discovered in outburst at 17.5 magnitudes (unfiltered, Balanutsa et al. 2014a). It was suspected to be eclipsing, and this was confirmed by observations at the Vatican Observatory (Garnavich & Kennedy 2014). We independently confirmed its eclipsing nature with *pt5m*. Very recently, Kennedy et al. (2016) published further photometric and spectroscopic
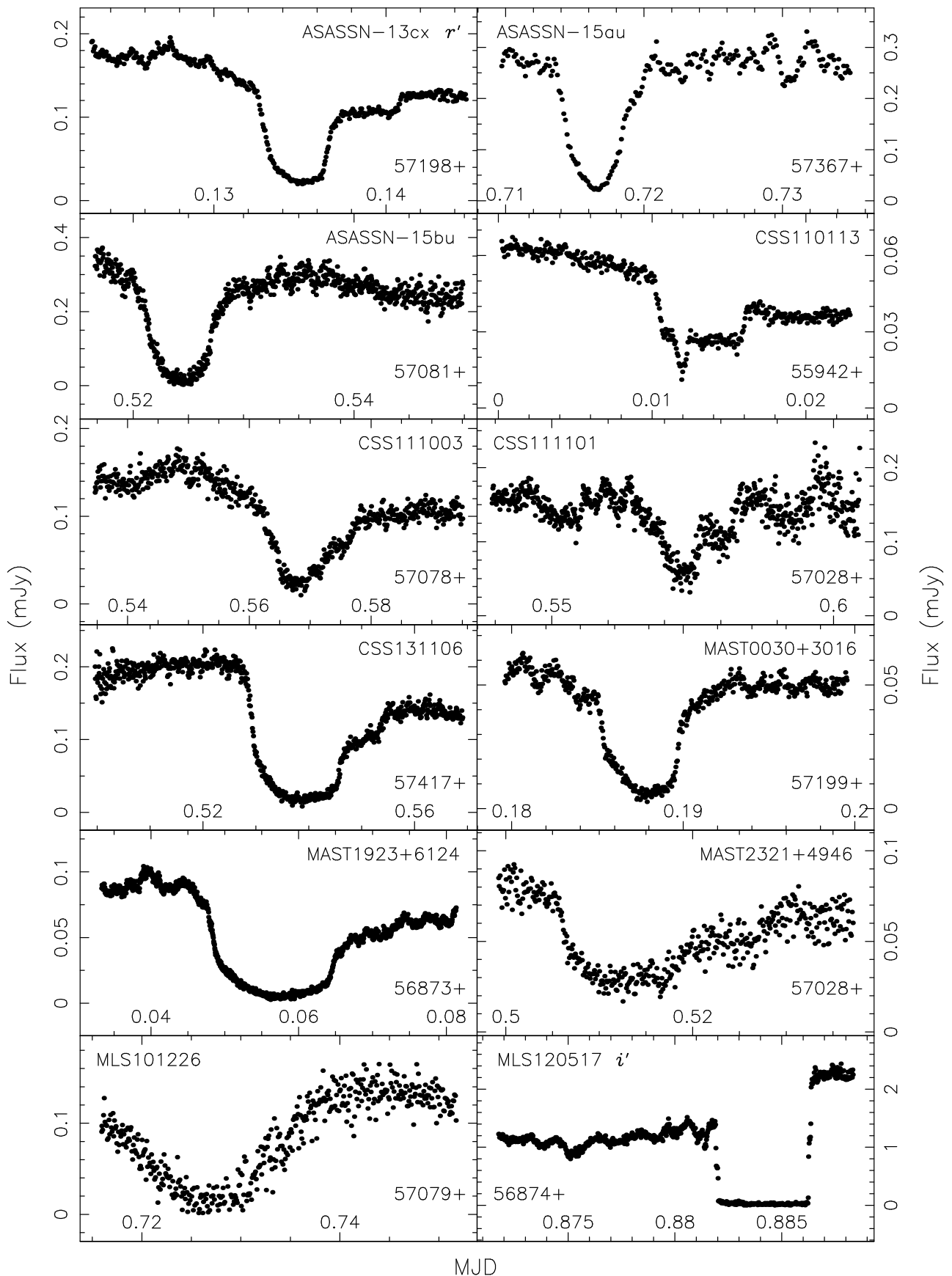
Figure 2. High-speed eclipses of newly discovered eclipsing systems, observed with ULTRACAM and ULTRASPEC. The instrument and filter used in each observation is given in Table B1. In the case of ULTRACAM observations, we plot the g'-band light curve unless otherwise indicated in the plot. See text for discussion of individual light curve morphology. In these light curves and all subsequent densely-sampled light curves, error bars have been omitted for clarity.

studies of this system, showing that it shares similarities with the SW Sex class of CVs during outburst. Similar to those of Kennedy et al. (2016), our quiescent eclipse observations show clearly the white dwarf ingress and egress, but no bright spot is present.

MASTER OT J232100.42+494614.0: Discovered via an outburst to 15.5 magnitudes (Shumkov et al. 2014b) from $V = 19$ magnitudes in quiescence. We found MASTER OT J232100.42+494614.0 to have a long period of over 5 hours. The high-speed eclipse is noisy, and although there are signs of bright spot features, better data is needed before we can judge conclusively the potential for modelling this system. This is a priority, as a system with such a long period would be particularly useful to the CV evolution studies, since measurements of system parameters at long periods remain scarce (Zorotovic, Schreiber & Gänsicke 2011).

MLS101226:072033+172437: Discovered by CRTS (Drake et al. 2009) with a MLS light curve showing obvious variability, which was interpreted as eclipses (Drake et al. 2014). However, no detailed studies have, to our knowledge, been published. We confirmed its eclipsing nature with *pt5m* and also observed MLS101226:072033+172437 with ULTRASPEC. Unfortunately observations began a little late, missing the beginning of eclipse ingress. The eclipse is smooth and dominated by the disk feature, showing no strong white dwarf or bright spot components.

MLS120517:152507-032655: Flagged as a possible MLS CV candidate in 2012, after also showing substantial variability in the CSS data as far back as 2007. The source has a quiescent magnitude of around $V=19$, but appears to have been brightening for several years and is now seen at $V\sim16$. The object, also known as 1RXS J152506.9-032647, is detected in X-rays and the UV (Voges et al. 1999). It was proposed to show deep eclipses by Drake et al. (2014), and although no further studies have been published on MLS120517:152507-032655, it has been observed by amateur astronomers[4] and does indeed show eclipses.

We made several observations of the system with *pt5m* and ULTRACAM, all of which show the system to be brighter after eclipse than before. This behaviour is typical for a polar CV (Hellier 2001), when the eclipse signal is primarily due to the obscuration of a hot spot on the surface of the white dwarf. Most of the light in the system comes from this hot spot where the accretion stream impacts the surface, and from the stream itself that trails between this spot and the L1 point on the donor star. The projection effect of this stream causes the system to appear bright just after the eclipse, when the stream is being viewed more side-on than before the eclipse. As a polar, the light curve is not suitable for modelling to determine the system parameters.

SSS130413:094551-194402: Long suspected of being a variable star, this system was first known as NSV4618 (Kukarkin et al. 1981). The Siding Springs Survey (SSS, part of CRTS) light curve also shows numerous faint measurements associated with eclipses. The *vsnet* collaboration reported eclipses and estimated an orbital period of 1.6 hours (alert 15615). We confirmed the eclipsing
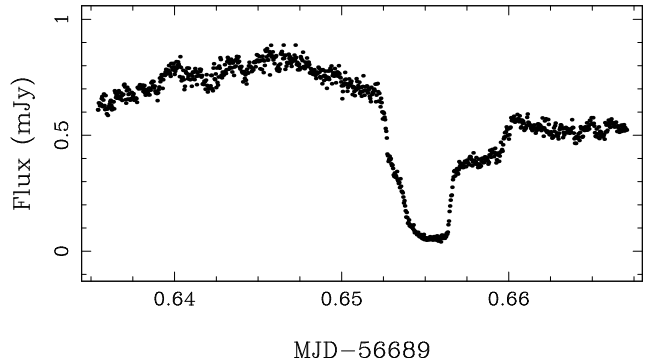
Figure 3. SSS130413:094551-194402 eclipse in the *KG5* filter, showing clearly separated white dwarf and bright spot features.

nature and Figure 3 shows the eclipse structure, which has clear white dwarf and bright spot features.

5 RESULTS: SYSTEMS NOT SHOWING ECLIPSES

The vast majority (>80%) of CV systems have orbital periods less than 5 hours (Ritter & Kolb 2003; Gänsicke et al. 2009). In addition, the eclipse duration tends to scale with the orbital period, such that longer period systems have longer eclipses. This means that a 5-hour observation showing no sign of eclipses would suggest the system either does not eclipse, or has a period of at least 5.5 hours. We can therefore say that any systems we have observed continuously for 5 or more hours that show no signs of eclipses are unlikely to be eclipsing.

Sometimes shorter observations can also help to rule out eclipses, if for example the system shows periodic variability. This could be due to superhumps, the projection effect of the orbiting bright spot, or the oblation of the secondary star as it fills its Roche lobe. These modulations occur on or close to the orbital period, thus any observation covering at least one cycle of such modulations without showing an eclipse is sufficient to rule out the presence of eclipses in the system.

In Table 2 we present 27 systems which did not show eclipses. We discuss and show light curves for only the two most interesting systems. Light curves of the other systems are given in Figures 1-25 in the supplementary online materials. Details of the observations are given in Table B1.

ASASSN-14mv: We observed ASASSN-14mv for two hours during outburst with ULTRASPEC. The light curve is shown in Figure 4, showing strong periodic variability associated with superhumps, suggesting an orbital period of the order of 40 minutes. This, along with other observations including *vsnet* alerts 18124 and 18160 (which links to an amateur spectrum taken by M. Potter showing helium absorption lines during outburst), suggests that ASASSN-14mv is likely to be an AM CVn system (Nelemans 2005).

CSS140402:173048+554518: This object, also known as SDSS J173047.59+554518.5 is a confirmed AM CVn system, with an orbital period of 35 minutes (Carter et al. 2014). Although not likely to be eclipsing due to it being a relatively face-on system, we observed CSS140402:173048+554518

Table 2. Summary of CVs not showing eclipses. Magnitudes given without filters are MASTER unfiltered magnitudes. SH = superhumps.

Object	Outburst Mag.	Quiescent Mag.	SH?	Approx. Period (mins)	Comments	References
ASASSN-14cl	V=10.7	g=18.8	Y	85		Stanek et al. 2014a; Kato et al. 2015
ASASSN-14ds	V=15.7	V=16.8	N		Known X-ray source	Holoien et al. 2014; Masetti et al. 2014
ASASSN-14gl	V=15.7	g=18.8	N		Flickering	
ASASSN-14gu	V=15.2	V=17.4	N	170	Periodic modulation	
ASASSN-14hk	V=14.7	B=20.8	Y	90		Stanek et al. 2014b; Kato et al. 2015
ASASSN-14mv	V=12	B=17.3	Y	40	Candidate AM CVn	Denisenko et al. 2014a
ASASSN-15ni	V=12.9	Unknown	N		Flickering	Dong et al. 2015; Berardi 2015
CSS090219:044027+023301	V=16.5	V=18.5	N		Flickering	Thorstensen & Skinner 2012
CSS091116:232551-014024	V=15.9	V=18.5	N		Flickering	Djorgovski et al. 2011
CSS100508:085604+322109	V=16.5	g=19.6	N		Flickering	Kato, Maehara & Uemura 2012
CSS100520:214426+222024	V=14.7	g=17.6	N			
CSS110114:091246-034916	V=16.0	R=18	N		Flickering	Thorstensen & Skinner 2012
CSS110226:112510+231036	V=16.0	R=19	N		Double-peaked lines	Kato, Maehara & Uemura 2012; Breedt et al. 2014
CSS130906:064726+491542	V=14	V=17	N		Also seen by MASTER	Tiurina et al. 2013; Thorstensen, Alper & Weil 2016
CSS140402:173048+554518	V=14.5	g=20.1	Y	39	Known AM CVn type	Carter et al. 2014; Kato et al. 2015
CSS140901:013309+133234	V=15.3	g=21.3	Y	150	A.K.A ASASSN-14gk	Kaur et al. 2014
CSS141005:023428-045431	V=14.5	g=16.3	Y	83	A.K.A ASASSN-14dx	Kaur et al. 2014; Thorstensen, Alper & Weil 2016
CSS141117:030930+263804	V=12	g=18.9	N			Kato et al. 2015
Gaia15aan	G=13	g=19.7	N		A.K.A ASASSN-14mo	Carter et al. 2013; Campbell et al. 2015
MAST034045.31+471632.2	15.6	g=18	N			Denisenko et al. 2013
MAST041923.57+653004.3	13.9	V=17.9	N		Known X-ray source	Balanutsa et al. 2013
MAST171921.40+640309.8	15.6	g=21.3	Y	80		Balanutsa et al. 2014b
MAST194955.17+455349.6	16.4	g=19.7	N		A.K.A KIC 9358280	Greiss et al. 2012; Denisenko et al. 2014c
MAST201121.95+565531.1	16.5	$R > 20$	N			Shurpakov et al. 2014b
MAST202157.69+212919.4	16.3	V=20	N		Known X-ray source	Voges et al. 2000; Denisenko et al. 2014b
MAST203421.90+120656.9	17.4	B=20.4	N			Yecheistov et al. 2014
MAST210316.39+314913.6	13.9	B=19.4	N			Shumkov et al. 2014a
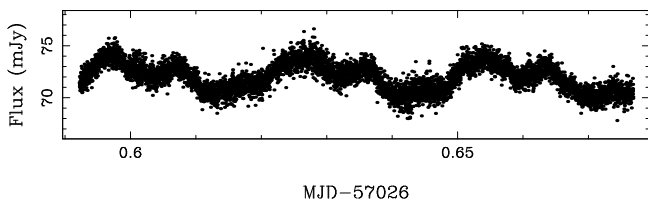
Figure 4. ASASSN-14mv light curve in the g' filter. The periodic modulation is associated with superhumps, and has a period of approximately 40 minutes. Error bars have been omitted for clarity.
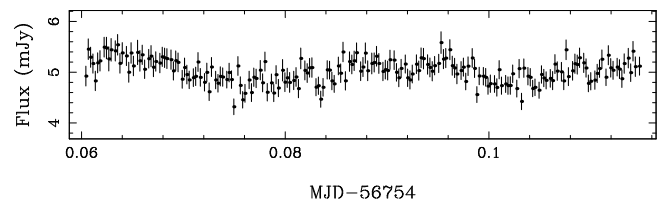
Figure 5. CSS140402:173048+554518 V-band light curve showing superhumps, observed during outburst.

6 RESULTS: PREVIOUSLY KNOWN ECLIPSING SYSTEMS

We present high cadence light curves of CV systems which are already known to be eclipsing. Studies at such high time resolution do not appear elsewhere in the literature, and therefore many of these systems have never been studied before in such detail. Some systems have already been studied in a time-resolved manner, but our additional observations should enable further refinement of existing measurements of system parameters. Details of the observations are given in Table B1, and mid-eclipse times are provided whenever an eclipse was observed. In those systems with resolved eclipse structure, we measure the mid-eclipse time as the mid point between the white

during outburst with automated follow-up from the initial CRTS transient trigger (Hardy et al. 2015). A 1.3 hour light curve is shown in Figure 5, showing superhump behaviour with a period of 39 minutes, close to the orbital period. This is also similar to the 35 minutes measured by Kato et al. (2015). Unfortunately, because of the large uncertainty in the spectroscopic orbital period, and since the accretion disk is made predominantly of helium and not hydrogen, the superhump excess cannot be reliably used to measure a mass ratio (Pearson 2007; Kato et al. 2014b), as can be done for classical SU UMa systems (Patterson et al. 2005).

dwarf mid-ingress and mid-egress, when these features are visible, rather than using a Gaussian fitting procedure. If the white dwarf ingress or egress is not clear but there is visible structure, we use the ingress and egress of the most consistent features, and account for this in the uncertainties. We derived updated ephemerides for most systems, and these are given in Table 3.

We provide discovery references and discuss the eclipse structure of each system below. Whether or not each system is suitable for light curve modelling to determine the system parameters is included in Table 3. Light curves for each system are shown in Figures 6, 7, 8 and 9.

1RXS J180834.7+101041: Originally classified as a polar (Denisenko, Kryachko & Satovskiy 2008), spectra later showed that it has an accretion disk (Bikmaev & Sakhibullin 2008). Eclipses have been studied previously (Yakin et al. 2010; Southworth & Copperwheat 2011), but attempts to measure the system parameters have had limited success because the white dwarf itself might not be eclipsed. We found strong flickering and only weak eclipse structure, possibly associated soley with the accretion disk and bright spot but not the white dwarf.

CSS080227:112634-100210: Discovered by CRTS (Drake et al. 2008; Djorgovski et al. 2008; Drake et al. 2009). The CSS light curve shows numerous dips due to eclipses, and these were later observed with time-resolved photometry (Woudt & Warner 2010). The eclipse displays a separated bright spot ingress and egress, although the egress is less clear due to flickering. Other eclipses show similar features, and with additional observations this system may be suitable for light curve modelling.

CSS080306:082655-000733: Discovered by CRTS. Photometry by Woudt et al. (2012) found eclipses and persistent negative superhumps, even in quiescence. Clear bright spot features are present.

CSS080623:140454-102702: Time-resolved photometry revealed eclipses (Woudt et al. 2012) and spectroscopy found both the white dwarf and the secondary star to be present in the spectrum (Breedt et al. 2014). This system shows classic CV eclipse structure with resolved white dwarf and bright spot features.

CSS081220:011614+092216: CSS found faint measurements signalling eclipses. Time-resolved photometry confirmed deep eclipses (Coppejans et al. 2014) and found an orbital period of around 1.6 hours. Most of our observations found either the bright spot ingress blended with that of the white dwarf, or the bright spot egress lost in flickering. Occasionally the system was found in a low-flickering state, with the bright spot features visible.

CSS090102:132536+210037: Numerous eclipse-like dips are visible in the CSS light curve. Also known as SDSS J132536.05+210036.7, it was flagged as a dwarf nova in retrospective data mining of SDSS objects by Wils et al. (2010) because of its strong blue colour (u'-g' of -1 magnitudes) an odd g'-r' colour (almost 3 magnitudes), which must have been affected by an eclipse. Southworth et al. (2015) studied the system in detail and confirmed its eclipsing nature. Most of our observations show resolved white dwarf and bright spot features.

CSS090419:162620-125557: This system is relatively faint in quiescence (r'=20.4) and all observations are noisy. Follow-up photometry identified eclipses (Woudt et al. 2012), and we have observed these at high speed. The light curve displays clear white dwarf and bright spot eclipses.

CSS090622:215636+193242: CSS light curve showed many dips suggestive of eclipses. The eclipsing nature was confirmed by Drake et al. (2014) and studied later by Thorstensen, Alper & Weil (2016). The high speed eclipse shows clear white dwarf and bright spot features.

CSS100218:043829+004016: Found to be eclipsing by Coppejans et al. (2014), who derived a period of 1.5 hours. The system is faint, with strong flickering and a weak bright spot.

CSS110513:210846-035031: Shows faint measurements in the long-term light curve, and Coppejans et al. (2014) confirmed eclipses with an orbital period of 3.8 hours. Unfortunately most of our observations found the system in outburst, showing an eclipse dominated by the disk. However, one high quality quiescent eclipse was observed, which showed separated white dwarf and bright spot features.

CSS111019:233313-155744: Found with a short period of around 62 minutes (Woudt & Warner 2011). The eclipses are shallow, and the bright spot eclipse appears to arrive very late - almost after the white dwarf has come out of eclipse. This behaviour is similar to that seen in the AM CVn system SDSS J092638.71+362402.4 (Marsh et al. 2007; Copperwheat et al. 2011), where the secondary star is so bright and small in size (e.g. a white dwarf), that the eclipses are shallow and the bright spot ingress occurs after the primary white dwarf egress. The short period also fits with a possible AM CVn classification. CSS111019:233313-155744 would be an interesting object for further study.

CzeV404 Her: Discovered in outburst by Cagas & Cagas (2014), and further studied by Bąkowska et al. (2014), who observed multiple super-outbursts and estimated an orbital period within the period gap. The bright spot and white dwarf ingresses appear to be blended, although there may be a hint of separation.

GALEX J003535.7+462353: Long-term variability in SuperWASP data (Butters et al. 2010) prompted time-resolved photometry which discovered dwarf novae outbursts and eclipses (Wils et al. 2011). Most of our observations showed little or no sign of bright spot features. Some distinct structure is visible in the eclipse light curve, but more observations are needed.

GY Cnc: Already has spectroscopically derived masses (Thorstensen 2000) and published ULTRACAM data (Feline et al. 2005). We found signs of a varying orbital period for this system, although since the system appears to have a variable disk radius, we cannot be certain we are always measuring the exact mid-eclipse time of the same features. The eclipse sometimes has clear bright spot features, though often we found these components blended with the white dwarf.

HS 2325+8205: Already studied extensively (Pyrzas et al. 2012), and found to be a candidate eclipsing Z Cam type CV, with a long orbital period. The eclipse appears to be
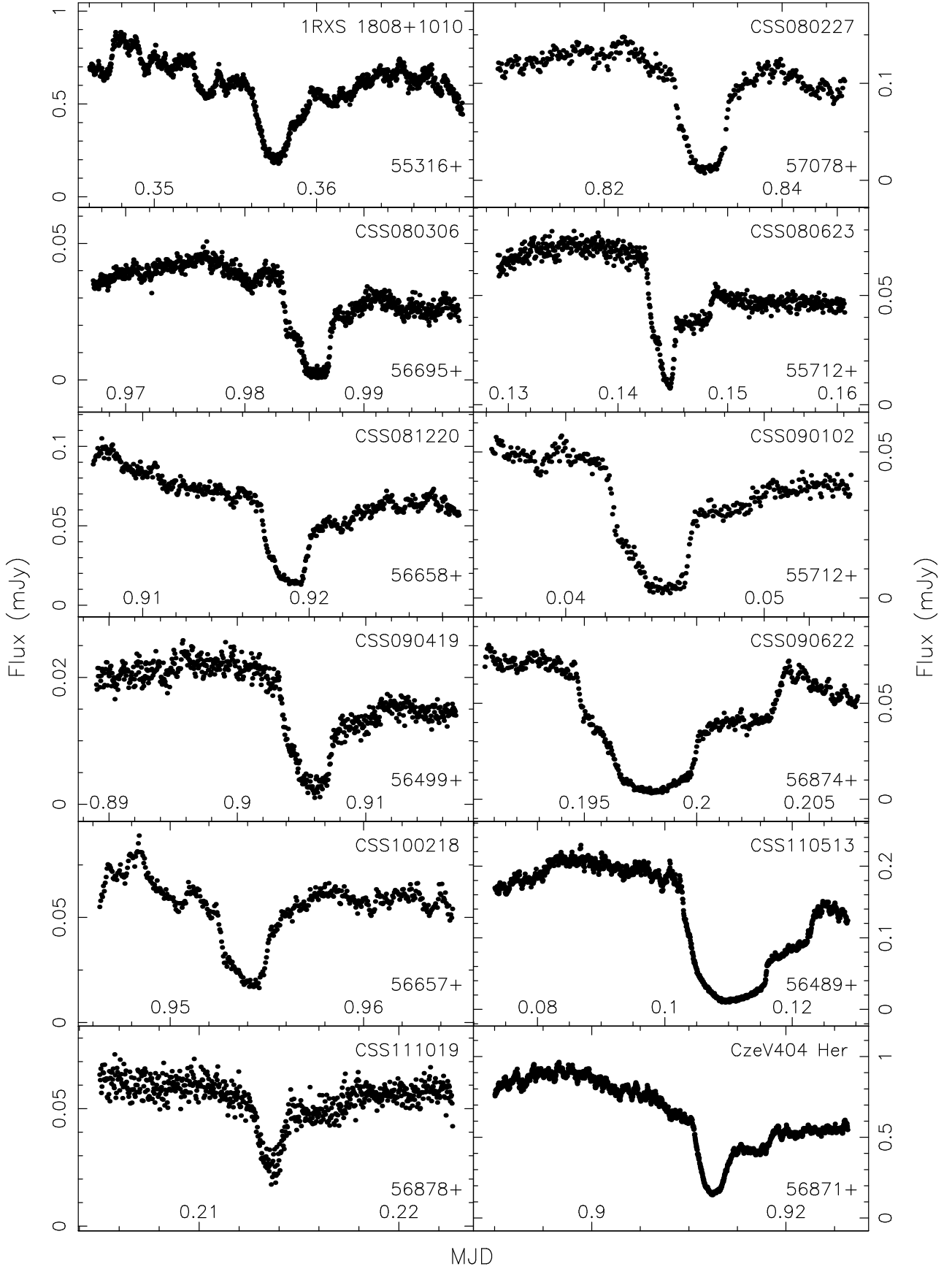
Figure 6. High-speed eclipses of known eclipsing systems, observed with ULTRACAM, ULTRASPEC and SALTICAM. The instrument and filter used in each observation is given in Table B1. The g'-band light curve is shown for all ULTRACAM observations. See text for discussion of individual light curve morphology.
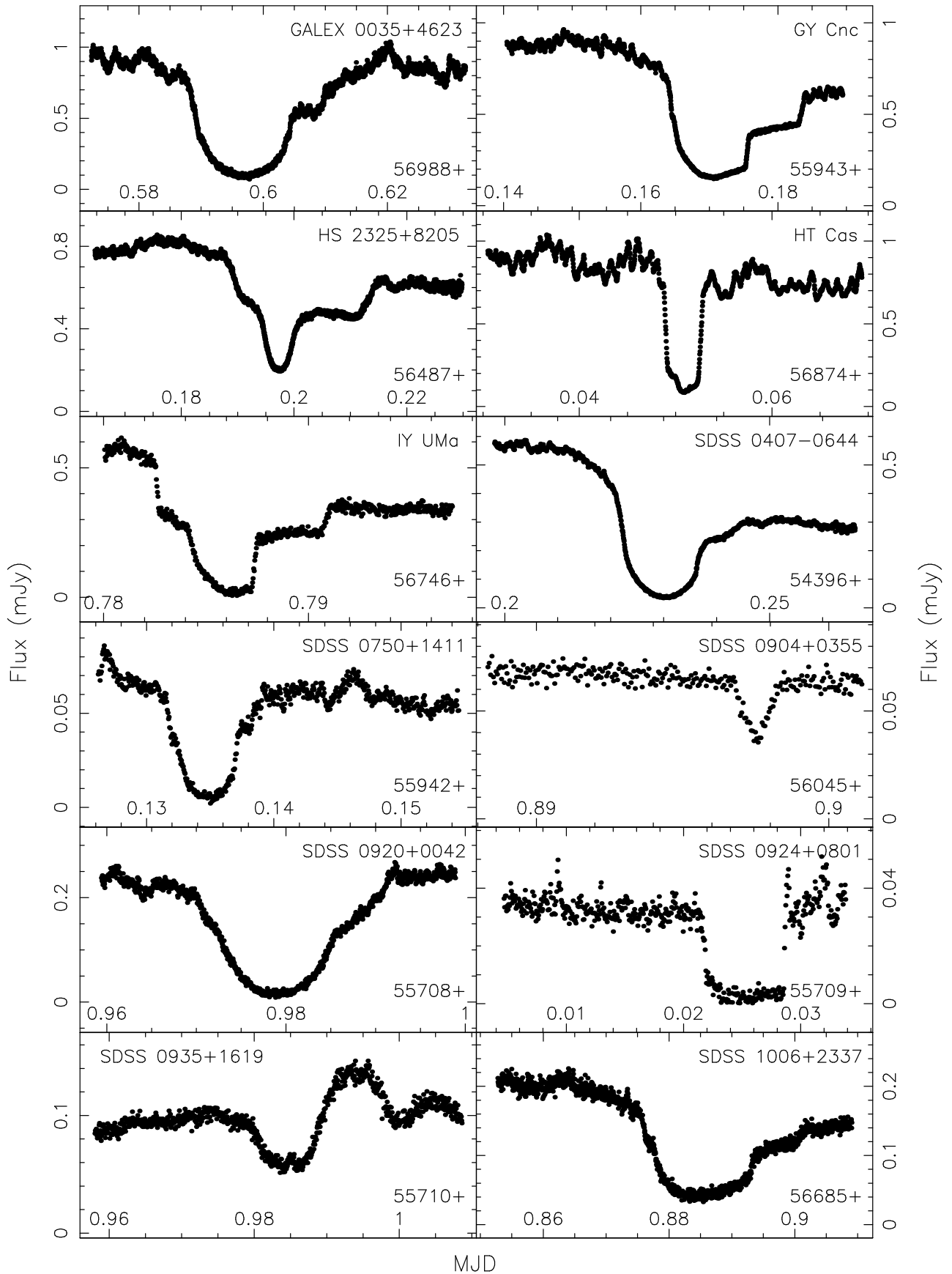
Figure 7. High-speed eclipses of known eclipsing systems, observed with ULTRACAM and ULTRASPEC. The instrument and filter used in each observation is given in Table B1. The g'-band light curve is shown for all ULTRACAM observations. See text for discussion of individual light curve morphology.

well suited for modelling with clearly visible white dwarf and bright spot features.

HT Cas: Well-studied (Horne, Wood & Stiening 1991) and observed with ULTRACAM before (Feline et al. 2005). There are signs of an evolving orbital period for this system according to the linear fit to the mid-eclipse times. This is discussed in detail in Bours et al. (2016). Normally HT Cas shows lots of flickering, and eclipses with no visible bright spot. For a short time in 2014 the bright spot ingress was visible, but with the egress masked by flickering.

IY UMa: Known to be eclipsing for many years (Uemura et al. 2000), IY UMa has been studied extensively (Steeghs et al. 2003). System parameter determinations already exist, but have large uncertainties.

SDSS J040714.78-064425.1: Also known as LT Eri, this system was discovered in SDSS follow up (Szkody et al. 2003). Further studies confirmed a period of around 4 hours (Ak et al. 2005), placing it well above the period gap. The CSS light curve shows many rapid ~2 magnitude outbursts. We often found the system in outburst, but even in quiescence it usually shows blended white dwarf and bright spot ingresses.

SDSS J075059.97+141150.1: Discovered in SDSS (Szkody et al. 2007) and shows frequent outbursts in its CSS light curve. Southworth et al. (2010) presented time-resolved photometry and were able to measure the system parameters through light curve modelling. However, these measurements suffered from high uncertainties due to the low cadence of the observations.

SDSS J090103.93+480911.1: Discovered in SDSS (Szkody et al. 2003), SDSS J090103.93+480911.1 has been studied photometrically already (Dillon et al. 2008; Shears et al. 2012; Kato et al. 2013). Our observations spanning 6 years found an evolution of bright spot features. At first the bright spot was clearly visible, then it disappeared and the flickering intensified. Later the flickering decreased and the bright spot returned. Two phase-folded light curves are shown in Figure 8 to demonstrate this behaviour.

SDSS J090403.49+035501.2: Discovered in SDSS (Szkody et al. 2004), and already studied photometrically (Woudt et al. 2012). It shows no outbursts in the CSS archival light curve. We observed a single eclipse of this system confirming the grazing nature of its eclipses, but the large orbital hump seen in other observations (Woudt et al. 2012) is not present. We cannot improve on the precision of the ephemeris in Woudt et al. (2012).

SDSS J092009.54+004245.0: Discovered in SDSS (Szkody et al. 2003), further studies revealed a period of 3.5 hours (Gänsicke et al. 2009; Zengin Çamurdan, İbanoğlu & Çamurdan 2010). It has since been suggested to be a SW Sex system (Schmidtobreick, Rodríguez-Gil & Gänsicke 2012), a nova-like with a strong, flared disk. We found that the eclipses have some structure, with a probable strong disk component, but without any clear sign of a white dwarf. This supports the SW Sex classification as a nova-like variable.

SDSS J092444.48+080150.9: Also known as HU Leo and discovered in SDSS spectra (Szkody et al. 2005). Numerous eclipses have been observed (Southworth et al. 2010, 2015), and we present one additional eclipse. The
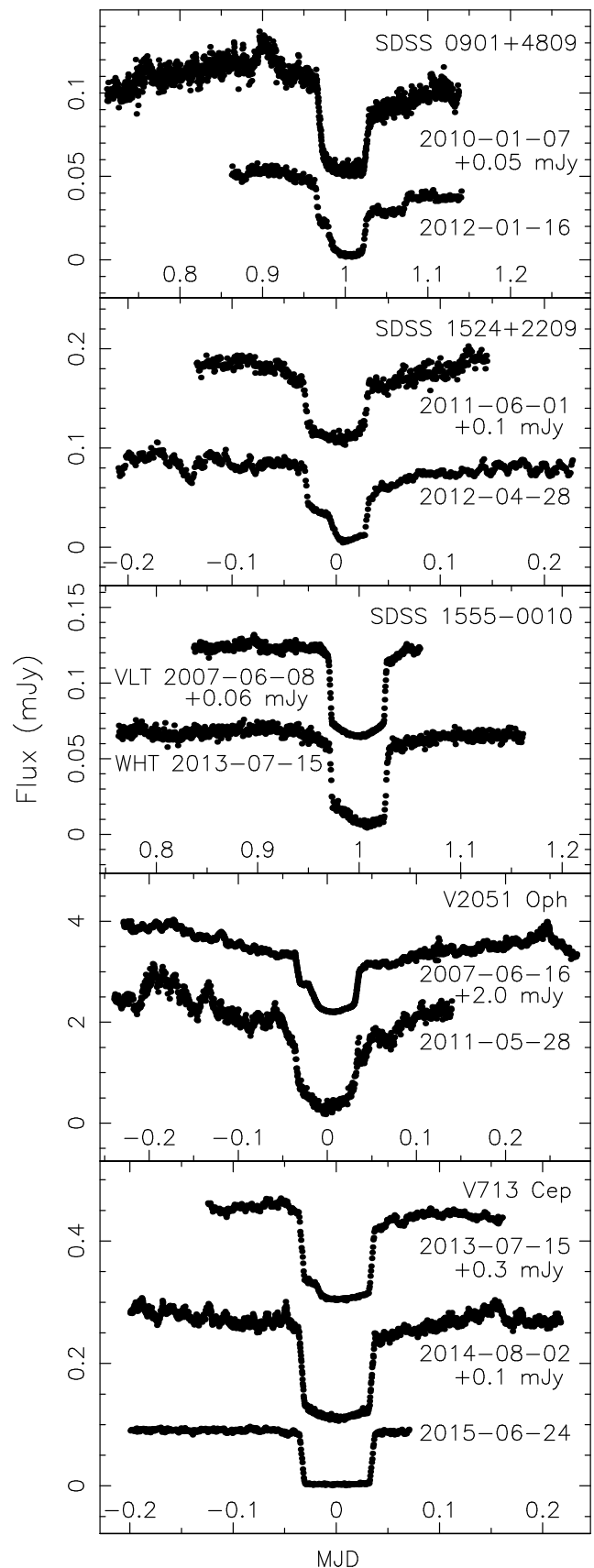
Figure 8. Phase-folded high-speed eclipses of known eclipsing systems showing variable bright spot features. Observations were conducted in g' with ULTRACAM. Individual eclipses have been offset vertically in each panel by the specified amount. See text for discussion of individual light curve morphology.

system shows no signs of an accretion disk, and has the possible characteristics of a polar light curve, showing a bright post-eclipse hump due to the projection effect of the accretion stream. We are unable to refine the ephemeris further.

SDSS J093537.46+161950.8: Discovered in SDSS (Szkody et al. 2009), with a spectrum that could have been classified as a polar or an old nova. It has also been studied photometrically (Southworth et al. 2015). We observed a single eclipse with ULTRACAM, finding a typical polar light curve similar to that seen in HU Aqr (Harrop-Allin et al. 1999).

SDSS J100658.40+233724.4: Discovered in SDSS (Szkody et al. 2007), this system has already been studied in detail. Southworth et al. (2009) published full system parameters based on time-resolved photometry and spectroscopy. We continued to observe SDSS J100658.40+233724.4 in an attempt to improve on these measurements. The eclipse light curve displays clear white dwarf and bright spot features, but some observations suffer from strong flickering.

SDSS J115207.00+404947.8: Time-resolved ULTRACAM observations already exist, with parameters determined through light curve modelling (Savoury et al. 2011). We later discovered that the ephemeris presented in Savoury et al. (2011) suffered from a cycle count ambiguity. We have since observed 4 more eclipses of this CV, and a new ephemeris is given in Table 3. The new eclipse observations have stronger bright spot features than previously seen.

SDSS J125023.84+665525.4: Also known as OV Dra, discovered with a high inclination in SDSS spectra (Szkody et al. 2003). The archival CSS light curve shows long-term variability, eclipse-like dips, and several outbursts. Time-resolved photometry confirmed eclipses (Dillon et al. 2008; Kato et al. 2014a), but no high-speed studies have been published so far. Our observations found the bright spot eclipse to be visible, but unfortunately it is often interrupted by flickering.

SDSS J152419.33+220920.1: Discovered in SDSS spectra (Szkody et al. 2009), which revealed double-peaked emission lines suggesting a high inclination. It was also independently discovered as a dwarf nova by CRTS and is therefore also known as CSS090329:152419+220920. Time-resolved photometry later revealed eclipses (Southworth et al. 2010), which were modelled to estimate the inclination and mass ratio of the system, but the data were not of sufficient quality to measure the individual component masses. Further photometry of 27 eclipses improved the ephemeris greatly (Michel, Echevarría & Hernández Santisteban 2013). In our first observations SDSS J152419.33+220920.1 showed minimal bright spot features, and often its eclipse was completely blended with that of the white dwarf. However, the disk radius and/or bright spot flux changed in later observations, showing a clear bright spot component which is separate from the white dwarf. Figure 8 shows two phase-folded eclipses which demonstrate this change in eclipse structure.

SDSS J155531.99-001055.0: Discovered in SDSS (Szkody et al. 2002), with double-peaked emission lines indicating a high inclination. The CSS light curve showed
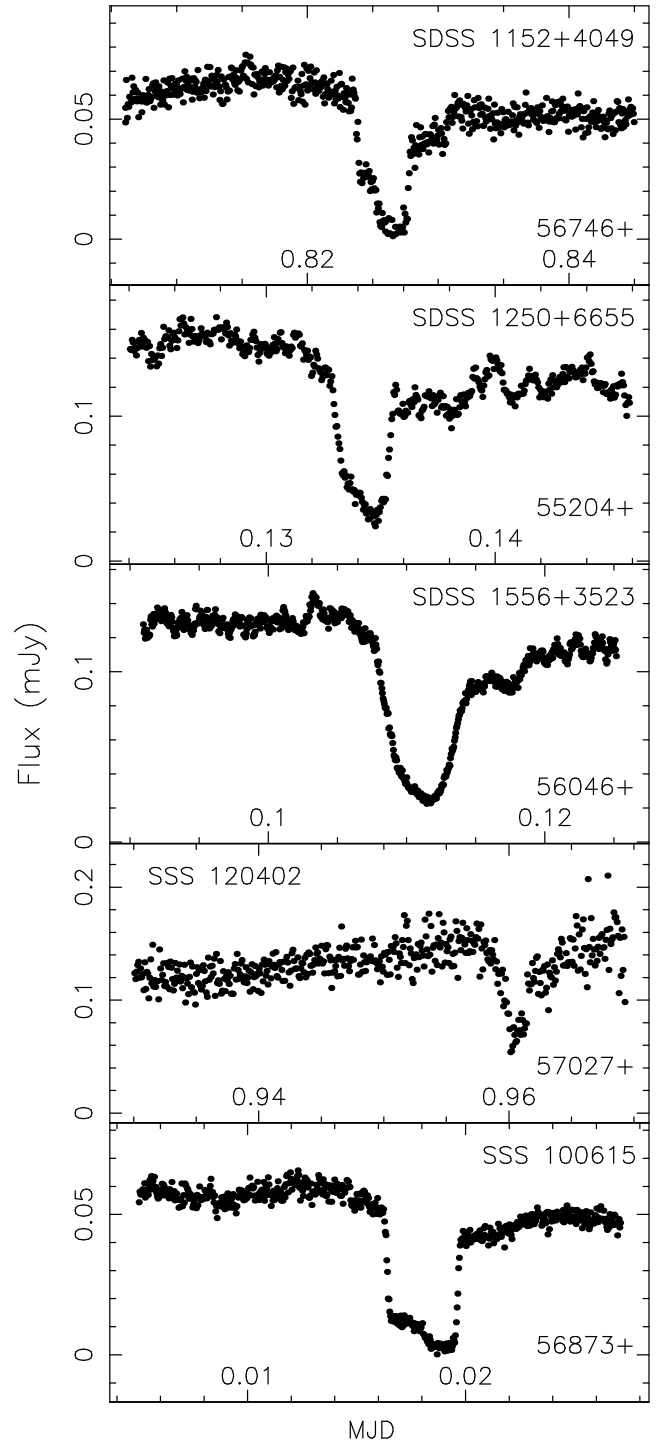
Figure 9. High-speed eclipses of known eclipsing systems, observed with ULTRACAM and ULTRASPEC. The instrument and filter used in each observation is given in Table B1. The g'-band light curve is shown for all ULTRACAM observations. See text for discussion of individual light curve morphology.

no outbursts, but does hint at eclipses with occasional faint measurements. Photometric follow-up confirmed the eclipses and an orbital period of 113 minutes (Southworth et al. 2007). The eclipse structure clearly changes over time, as shown in Figure 8. In 2007 there were no bright spot

features, but in 2013 the bright spot ingress, at least, is clear.

SDSS J155656.92+352336.6: Also known as BT CrB, discovered with an orbital period of around 2 hours in SDSS (Szkody et al. 2006). High cadence observations of the eclipse often show the white dwarf and bright spot egresses well separated, but with blended ingresses. On one occasion the ingresses are marginally separated. Clearly this system has a variable disk radius, and at times could present an eclipse structure that can be modelled.

SSS100615:200331-284941: Discovered via an outburst in CRTS, and later observed by Coppejans et al. (2014). They found deep eclipses and an orbital period of 1.4 hours. Our observations show clearly visible bright spot features.

SSS120402:134015-350512: Discovered by CRTS showing multiple dwarf nova outbursts in its archival light curve, as well as fainter observations associated with eclipses. Coppejans et al. (2014) observed two eclipses, and derived a period of 1.4 hours. We observed a single eclipse with ULTRASPEC and confirm the eclipse is only partial in nature, with the eclipse of the white dwarf suspected to be grazing. We cannot improve on the ephemeris due to cycle count ambiguities.

V2051 Oph: Originally discovered on objective prism plates (Sanduleak 1972). It was studied photometrically by Warner & Cropper (1983), who found bright spot features, making this system a good target for eclipse modelling. V2051 Oph has been the subject of numerous studies, via eclipse mapping and Doppler tomography (Vrielmann, Stiening & Offutt 2002; Baptista & Bortoletto 2004; Saito & Baptista 2006; Longa-Peña, Steeghs & Marsh 2015), as well as eclipse-timing observations which show it has cyclical period changes and a larger than expected orbital decay rate (Baptista et al. 2003; Qian et al. 2015) - this may be due to the presence of a third body and/or magnetic braking. In the hope of being able to model the eclipse structure of V2051 Oph, we have observed a total of 26 high-speed eclipses over 8 years (Table B1). On many occasions the light curves are not useful, due to either cloudy conditions, the system being in outburst, the presence of strong flickering, or the bright spot eclipse not being visible. However, several observations appear to be useful, with visible bright spot features. Figure 8 shows two phase-folded eclipses showing the differences in eclipse structure at different epochs. We confirm the period changes discussed by Baptista et al. (2003) and Qian et al. (2015), though we cannot confirm that these changes are cyclical in nature due to the relatively short baseline of our observations.

V713 Cep: Originally discovered as variable by inspection of archival photometric plates (Antipin & Kroll 2003), eclipses were soon discovered in this CV (*vsnet* alert 9516). More detailed photometry showed that it had the classic CV eclipse structure that lends itself to light curve modelling (Boyd et al. 2011). There are signs of a varying orbital period for this system according to our linear fit to the mid-eclipse times. This is discussed in detail in Bours et al. (2016). We observed the bright spot in V713 Cep changing significantly over time. In some observations it is clearly seen, and in others there is no bright spot feature at all. The top two light curves in the bottom panel of Figure 8 demonstrate this.

In addition to this, we also observed an apparent complete switch-off of accretion on 2015-06-24. This eclipse, the bottom light curve shown in the bottom panel of Figure 8, is typical of detached binaries in which the white dwarf primary is not accreting gas from the secondary star. Three months later, on 2015-09-17, the system appeared to be accreting again. This low-state behaviour is unexpected and very rare among non-magnetic dwarf novae. The only other example of this was seen in IR Com, with an extended low state in which accretion was confirmed to have switched off (Manser & Gänsicke 2014). Low states are however found in the VY Scl class of nova-like variables, in both magnetic and non-magnetic systems (Hellier 2001).

One theory for temporary interruptions to mass transfer is that they occur when a starspot crosses the L1 point on the donor star, lowering the stellar surface and disconnecting it from the L1 point. In CVs with strong magnetic fields (i.e. polars), accretion onto the white dwarf ceases immediately, and the system enters a low state until mass transfer resumes. However, in non-magnetic dwarf novae the system remains bright, as the accretion disk is thought to outlive the short break in mass transfer, only draining slowly onto the white dwarf (Hessman 2000; Manser & Gänsicke 2014).

Our observations of V713 Cep show that this break in mass transfer is not constrained to nova-likes, polars and the single instance of IR Com, but may be more common than first thought. Unfortunately V713 Cep is not covered in the CSS footprint, and we cannot say exactly how long the low state lasted. Our observations of eclipses before and after the non-accreting observation on 2015-06-24 both show normal eclipse structure including an accretion disk. These are separated by 403 days and thus we constrain the low state of V713 Cep to a maximum duration of 403 days.

7 CONCLUSIONS

We have presented time-resolved photometry of 74 CVs, most of which have never before been observed in detail. We have discovered or confirmed 13 new eclipsing systems with orbital periods ranging from 1.5 to 5.1 hours. We studied 27 new systems which did not show any eclipses. The remaining 34 systems presented here were already known to be eclipsing, but we provide the highest cadence observations of these objects to date. For all eclipsing systems we have discussed the feasibility of modelling their eclipse structure to determine their system parameters. We found that approximately 20 of the objects discussed above should be suitable for system parameter studies using light curve modelling, while a further 15 systems may be feasibly modelled if additional observations are acquired.

Table 3. Ephemerides and suitability for modelling of eclipsing systems. Ephemerides are measured and quoted in BMJD(TDB). Some ephemerides have been calculated using additional mid-eclipse times from the literature. In these cases the relevant references are supplied. Where we have been unable to refine the ephemeris, we refer the reader to previous papers rather than repeating it here. Evaluation of the potential for light curve modelling is given as 'Y' for yes, 'N' for no, and 'M' for maybe/more data are needed.

Object	T_0	P	Additional Eclipse Times	Modelling Potential
1RXS J180834.7+101041	54926.3108(1)	0.06949063(5)	Southworth & Copperwheat 2011	N
ASASSN-13cx	57104.30636(1)	0.07965006(1)	-	M
ASASSN-15au	57148.04781(4)	0.06894973(2)	-	M
ASASSN-15bu	57080.98512(1)	0.0768262(9)	-	M
CSS080227:112634-100210	56294.94350(3)	0.077421572(3)	Southworth et al. 2015	M
CSS080306:082655-000733	56444.203767(8)	0.059764424(1)	-	Y
CSS080623:140454-102702	55488.728318(8)	0.059578972(2)	-	Y
CSS081220:011614+092216	56713.570050(8)	0.065843019(3)	Coppejans (priv.comm.)	M
CSS090102:132536+210037	56207.945385(5)	0.0623849134(7)	Southworth et al. 2015	Y
CSS090419:162620-125557	56551.813968(9)	0.075442719(5)	-	Y
CSS090622:215636+193242	56877.82014(2)	0.0709293(2)	-	Y
CSS100218:043829+004016	56658.417503(1)	0.0654948(1)	-	M
CSS110113:043112-031452	56396.181193(3)	0.0660508721(6)	-	Y
CSS110513:210846-035031	56767.65993(3)	0.15692657(3)	-	Y
CSS111003:054558+022106	56852.23197(9)	0.12097138(4)	Miszalski et al. 2016	Y
CSS111019:233313-155744	56866.13556(2)	0.04285020(1)	-	M
CSS111101:233003+303301	57015.4708(2)	0.1559784(6)	-	N
CSS131106:052412+004148	57126.37256(2)	0.17466647(2)	-	M
CzeV404 Her	56871.91730(4)	0.09802125(2)	-	M
GALEX J003535.7+462353	56489.69294(4)	0.17227491(1)	Wils et al. 2011	M
GY Cnc	55938.26369(1)	0.175442402(1)	Kato, Ishioka & Uemura 2002	Y
HS 2325+8205	55661.080122(7)	0.194334533(1)	Pyrzas et al. 2012	Y
HT Cas	55550.16974(3)	0.073647175(1)	Feline et al. 2005	N
IY UMa	54679.998816(9)	0.0739089285(3)	Steeghs et al. 2003	Y
MAST003059.39+301634.3	57159.48849(5)	0.07026247(3)	-	M
MAST192328.22+612413.5	56852.10211(9)	0.1676465(3)	Kennedy et al. 2016	N
MAST232100.42+494614.0	57010.6753(1)	0.2123715(9)	-	M
MLS101226:072033+172437	57023.1777(2)	0.1504066(3)	-	N
MLS120517:152507-032655	56821.89967(5)	0.06438163(7)	-	N
SDSS J040714.78-064425.1	56332.1340(1)	0.17020393(2)	-	N
SDSS J075059.97+141150.1	56306.51099(1)	0.093165496(2)	Southworth et al. 2010, 2015	Y
SDSS J090103.93+480911.1	55229.666015(7)	0.0778805326(6)	-	Y
SDSS J090403.49+035501.2	-	-	-	N
SDSS J092009.54+004245.0	56145.35967(3)	0.147875676(7)	-	N
SDSS J092444.48+080150.9	-	-	-	N
SDSS J093537.46+161950.8	55670.30839(6)	0.06405514(3)	Southworth et al. 2015	N
SDSS J100658.40+233724.4	56396.98203(6)	0.18591303(2)	Southworth et al. 2009, 2015	Y
SDSS J115207.00+404947.8	56082.544698(2)	0.0677497017(2)	Southworth et al. 2010; Savoury et al. 2011	Y
SDSS J125023.84+665525.4	54614.43088(1)	0.0587356818(6)	Dillon et al. 2008	M
SDSS J152419.33+220920.1	56287.823054(3)	0.0653187310(8)	Southworth et al. 2010	Y
SDSS J155531.99-001055.0	55267.794254(4)	0.0788455518(3)	Southworth et al. 2007	M
SDSS J155656.92+352336.6	55633.75890(3)	0.088091490(4)	-	M
SSS100615:200331-284941	56874.0223924(8)	0.05870445(6)	-	Y
SSS120402:134015350512	-	-	-	N
SSS130413:094551-194402	56809.688700(9)	0.065769292(3)	-	Y
V2051 Oph	55314.156237(4)	0.06242785751(8)	Vrielmann, Stiening & Offutt 2002; Baptista et al. 2003; Qian et al. 2015	Y
V713 Cep	56532.192754(5)	0.085418509(1)	-	Y

This work was based in part on observations made with *pt5m*, a collaborative effort between the Universities of Durham and Sheffield. Other observations have been made with telescopes operated by the Isaac Newton Group in La Palma, the National Astronomical Research Institute of Thailand, the European Southern Observatory in Chile,

and the South African Astronomical Observatory. This work has made use of NASA's Astrophysics Data System Bibliographic Services, the Vizier database operated at CDS, Strasbourg, France, and the International Variable Star Index (VSX) database operated at AAVSO, Cambridge, Massachusetts, USA.

REFERENCES

Ahn C. P. et al., 2012, ApJS, 203, 21

Ak T., Retter A., Liu A., Esenoğlu H. H., 2005, PASA, 22, 105

Antipin S. V., Kroll P., 2003, Information Bulletin on Variable Stars, 5461

Balanutsa P. et al., 2013, The Astronomer's Telegram, 5688, 1

Balanutsa P. et al., 2014a, The Astronomer's Telegram, 6097, 1

Balanutsa P. et al., 2014b, The Astronomer's Telegram, 5974, 1

Baptista R., Borges B. W., Bond H. E., Jablonski F., Steiner J. E., Grauer A. D., 2003, MNRAS, 345, 889

Baptista R., Bortoletto A., 2004, AJ, 128, 411

Bąkowska K., Olech A., Pospieszyński R., Martinelli F., Marciniak A., 2014, Acta Astron., 64, 337

Bell C. P. M., Naylor T., Mayne N. J., Jeffries R. D., Littlefair S. P., 2012, MNRAS, 424, 3178

Berardi P., 2015, The Astronomer's Telegram, 7854

Bikmaev I. F., Sakhibullin N. A., 2008, The Astronomer's Telegram, 1648

Blagorodnova N., Van Velzen S., Harrison D. L., Koposov S., Mattila S., Campbell H., Walton N. A., Wyrzykowski Ł., 2016, MNRAS, 455, 603

Bours M. C. P. et al., 2016, ArXiv e-prints, 1606.00780

Boyd D., Denisenko D., Koff R., Miller I., Staels B., 2011, Journal of the British Astronomical Association, 121, 233

Breedt E. et al., 2014, MNRAS, 443, 3174

Butters O. W. et al., 2010, A&A, 520, L10

Cagas P., Cagas P., 2014, Information Bulletin on Variable Stars, 6097, 1

Campbell H. et al., 2015, The Astronomer's Telegram, 7177, 1

Carter P. J. et al., 2013, MNRAS, 429, 2143

Carter P. J., Steeghs D., Marsh T. R., Kupfer T., Copperwheat C. M., Groot P. J., Nelemans G., 2014, MNRAS, 437, 2894

Castelli F., Kurucz R. L., 2004, ArXiv e-prints, 0405087

Coppejans D. L. et al., 2014, MNRAS, 437, 510

Copperwheat C. M. et al., 2011, MNRAS, 410, 1113

Copperwheat C. M. et al., 2012, MNRAS, 421, 149

Denisenko D. et al., 2014a, The Astronomer's Telegram, 6857, 1

Denisenko D. et al., 2014b, The Astronomer's Telegram, 6328, 1

Denisenko D. et al., 2014c, The Astronomer's Telegram, 6325, 1

Denisenko D. et al., 2013, The Astronomer's Telegram, 5698, 1

Denisenko D. V., Kryachko T. V., Satovskiy B. L., 2008, The Astronomer's Telegram, 1640

Dhillon V. S. et al., 2014, MNRAS, 444, 4009

Dhillon V. S. et al., 2007, MNRAS, 378, 825

Dillon M. et al., 2008, MNRAS, 386, 1568

Djorgovski S. G. . et al., 2008, The Astronomer's Telegram, 1416

Djorgovski S. G. et al., 2011, ArXiv e-prints, 1102.5004

Dong S. et al., 2015, The Astronomer's Telegram, 7850

Dotter A., Chaboyer B., Jevremović D., Kostov V., Baron E., Ferguson J. W., 2008, ApJS, 178, 89

Drake A. J. et al., 2009, ApJ, 696, 870

Drake A. J. et al., 2014, MNRAS, 441, 1186

Drake A. J., Williams R., Mahabal A., Djorgovski S. G., Graham M. J., Beshore E. C., Larson S. M., Christensen E., 2008, The Astronomer's Telegram, 1399

Feline W. J., Dhillon V. S., Marsh T. R., Watson C. A., Littlefair S. P., 2005, MNRAS, 364, 1158

Fukugita M., Yasuda N., Doi M., Gunn J. E., York D. G., 2011, AJ, 141, 47

Gänsicke B. T. et al., 2009, MNRAS, 397, 2170

Garnavich P., Kennedy M., 2014, The Astronomer's Telegram, 6116, 1

Greiss S. et al., 2012, AJ, 144, 24

Gunn J. E., Stryker L. L., 1983, ApJS, 52, 121

Hardy L. K., Butterley T., Dhillon V. S., Littlefair S. P., Wilson R. W., 2015, MNRAS, 454, 4316

Harrop-Allin M. K., Cropper M., Hakala P. J., Hellier C., Ramseyer T., 1999, MNRAS, 308, 807

Hellier C., 2001, Cataclysmic Variable Stars. Springer-Praxis, New York

Hessman F. V., 2000, New Astron. Rev., 44, 155

Holoien T. W.-S. et al., 2014, The Astronomer's Telegram, 6306, 1

Horne K., Wood J. H., Stiening R. F., 1991, ApJ, 378, 271

Jacoby G. H. et al., 2010, PASA, 27, 156

Kato T. et al., 2015, ArXiv e-prints, 1507.05610

Kato T. et al., 2013, PASJ, 65, 23

Kato T. et al., 2014a, PASJ, 66, 30

Kato T., Ishioka R., Uemura M., 2002, PASJ, 54, 1023

Kato T., Maehara H., Uemura M., 2012, PASJ, 64, 63

Kato T. et al., 2014b, PASJ, 66, L7

Kato T., Uemura M., Ishioka R., Nogami D., Kunjaya C., Baba H., Yamaoka H., 2004, PASJ, 56, S1

Kaur A., Porter A., Wilber A., Wagner R. M., Woodward C. E., Starrfield S. G., Hartmann D. H., 2014, The Astronomer's Telegram, 6624, 1

Kennedy M. R. et al., 2016, ArXiv e-prints, 1604.05718

Knigge C., 2006, MNRAS, 373, 484

Knigge C., Baraffe I., Patterson J., 2011, ApJS, 194, 28

Kukarkin B. V. et al., 1981, in Moscow, Acad. of Sciences USSR Sternberg, Vol. 1

Lasota J.-P., 2001, New Astron. Rev., 45, 449

Lipunov V. et al., 2010, Advances in Astronomy, 30, 349171

Littlefair S. P., Dhillon V. S., Marsh T. R., Gänsicke B. T., Southworth J., Baraffe I., Watson C. A., Copperwheat C., 2008, MNRAS, 388, 1582

Longa-Peña P., Steeghs D., Marsh T., 2015, MNRAS, 447, 149

Manser C. J., Gänsicke B. T., 2014, MNRAS, 442, L23

Marsh T. R. et al., 2007, in Astronomical Society of the Pacific Conference Series, Vol. 372, 15th European Workshop on White Dwarfs, Napiwotzki R., Burleigh M. R., eds., p. 431

Masetti N., Chavushyan V., Torrealba J., Jimenez-Bailon E., 2014, The Astronomer's Telegram, 6588, 1

McAllister M. J. et al., 2016, ArXiv e-prints, 1609.06143

Michel R., Echevarría J., Hernández Santisteban J. V., 2013, A&A, 554, A25

Miszalski B., Corradi R. L. M., Jones D., Santander-García M., Rodríguez-Gil P., Rubio-Díez M. M., 2011, in Asymmetric Planetary Nebulae 5 Conference, Zijlstra A. A., Lykou F., McDonald I., Lagadec E., eds.

Miszalski B. et al., 2016, MNRAS, 456, 633

Monet D. G. et al., 2003, AJ, 125, 984

Naylor T., 1998, MNRAS, 296, 339

Nelemans G., 2005, in Astronomical Society of the Pacific Conference Series, Vol. 330, The Astrophysics of Cataclysmic Variables and Related Objects, Hameury J.-M., Lasota J.-P., eds., p. 27

Nelemans G., Siess L., Repetto S., Toonen S., Phinney E. S., 2016, ApJ, 817, 69

O'Donoghue et al D., 2006, MNRAS, 372, 151

Osaki Y., 1996, PASP, 108, 39

Parsons S. G. et al., 2010, MNRAS, 407, 2362

Patterson J. et al., 2005, PASP, 117, 1204

Patterson J. et al., 2013, MNRAS, 434, 1902

Pearson K. J., 2007, MNRAS, 379, 183

Pickles A. J., 1998, PASP, 110, 863

Pyrzas S. et al., 2012, PASP, 124, 204

Qian S. B., Han Z. T., Fernández Lajús E., Zhu L. Y., Li L. J., Liao W. P., Zhao E. G., 2015, ApJS, 221, 17

Ritter H., Kolb U., 2003, A&A, 404, 301, (Update RKcat 7.23, 2015)

Saito R. K., Baptista R., 2006, AJ, 131, 2185

Sanduleak N., 1972, Information Bulletin on Variable Stars, 663

Savoury C. D. J. et al., 2011, MNRAS, 415, 2025

Savoury C. D. J., Littlefair S. P., Marsh T. R., Dhillon V. S., Parsons S. G., Copperwheat C. M., Steeghs D., 2012, MNRAS, 422, 469

Schenker K., King A. R., 2002, in Astronomical Society of the Pacific Conference Series, Vol. 261, The Physics of Cataclysmic Variables and Related Objects, Gänsicke B. T., Beuermann K., Reinsch K., eds., p. 242

Schmidtobreick L., Rodríguez-Gil P., Gänsicke B. T., 2012, Mem. Soc. Astron. Ital., 83, 610

Schreiber M. R., Zorotovic M., Wijnen T. P. G., 2016, MNRAS, 455, L16

Shappee B. J. et al., 2014, ApJ, 788, 48

Shears J., Hambsch F.-J., Littlefield C., Miller I., Morelle E., Pickard R., Pietz J., Sabo R., 2012, ArXiv e-prints, 1209.4062

Shumkov V. et al., 2014a, The Astronomer's Telegram, 6117, 1

Shumkov V. et al., 2014b, The Astronomer's Telegram, 6130

Shurpakov S. et al., 2014a, The Astronomer's Telegram, 5774, 1

Shurpakov S. et al., 2014b, The Astronomer's Telegram, 6257, 1

Smith D. A., Dhillon V. S., 1998, MNRAS, 301, 767

Southworth J., Copperwheat C. M., 2011, The Observatory, 131, 66

Southworth J., Copperwheat C. M., Gänsicke B. T., Pyrzas S., 2010, A&A, 510, 100

Southworth J., Hickman R. D. G., Marsh T. R., Rebassa-Mansergas A., Gänsicke B. T., Copperwheat C. M., Rodríguez-Gil P., 2009, A&A, 507, 929

Southworth J., Marsh T. R., Gänsicke B. T., Aungwerojwit A., Hakala P., de Martino D., Lehto H., 2007, MNRAS, 382, 1145

Southworth J., Tappert C., Gänsicke B. T., Copperwheat C. M., 2015, A&A, 573, 61

Stanek K. Z. et al., 2014a, The Astronomer's Telegram, 6233, 1

Stanek K. Z. et al., 2014b, The Astronomer's Telegram, 6479, 1

Steeghs D., Perryman M. A. C., Reynolds A., de Bruijne J. H. J., Marsh T., Dhillon V. S., Peacock A., 2003, MNRAS, 339, 810

Stellingwerf R. F., 1978, ApJ, 224, 953

STScI Development Team, 2013, pysynphot: Synthetic photometry software package. Astrophysics Source Code Library

Szkody P. et al., 2002, AJ, 123, 430

Szkody P. et al., 2011, AJ, 142, 181

Szkody P. et al., 2009, AJ, 137, 4011

Szkody P. et al., 2003, AJ, 126, 1499

Szkody P. et al., 2006, AJ, 131, 973

Szkody P. et al., 2004, AJ, 128, 1882

Szkody P. et al., 2005, AJ, 129, 2386

Szkody P. et al., 2007, AJ, 134, 185

Thorstensen J. R., 2000, PASP, 112, 1269

Thorstensen J. R., Alper E. H., Weil K. E., 2016, ArXiv e-prints, 1609.02215

Thorstensen J. R., Skinner J. N., 2012, AJ, 144, 81

Tiurina N. et al., 2013, The Astronomer's Telegram, 4871, 1

Tulloch S. M., Rodríguez-Gil P., Dhillon V. S., 2009, MNRAS, 397, L82

Uemura M. et al., 2000, PASJ, 52, L9

Voges W. et al., 1999, A&A, 349, 389

Voges W. et al., 2000, IAU Circular, 7432, 1

Vrielmann S., Stiening R. F., Offutt W., 2002, MNRAS, 334, 608

Warner B., 1995, Cataclysmic Variable Stars. Cambridge University Press, Cambridge

Warner B., Cropper M., 1983, MNRAS, 203, 909

Whitehurst R., 1988, MNRAS, 232, 35

Wijnen T. P. G., Zorotovic M., Schreiber M. R., 2015, A&A, 577, A143

Wils P., Gänsicke B. T., Drake A. J., Southworth J., 2010, MNRAS, 402, 436

Wils P., Krajci T., Hambsch F.-J., Muyllaert E., 2011, Information Bulletin on Variable Stars, 5982

Wood J. H., Horne K., Berriman G., Wade R., O'Donoghue D., Warner B., 1986, MNRAS, 219, 629

Woudt P. A., Warner B., 2010, MNRAS, 403, 398

Woudt P. A., Warner B., 2011, The Astronomer's Telegram, 3705

Woudt P. A., Warner B., de Budé D., Macfarlane S., Schurch M. P. E., Zietsman E., 2012, MNRAS, 421, 2414

Wu Z.-Y., Zhou X., Ma J., Du C.-H., 2009, MNRAS, 399, 2146

Wyrzykowski L., Hodgkin S., Blogorodnova N., Koposov S., Burgon R., 2012, ArXiv e-prints, 1210.5007

Yakin D. G., Suleimanov V. F., Shimansky V. V., Borisov
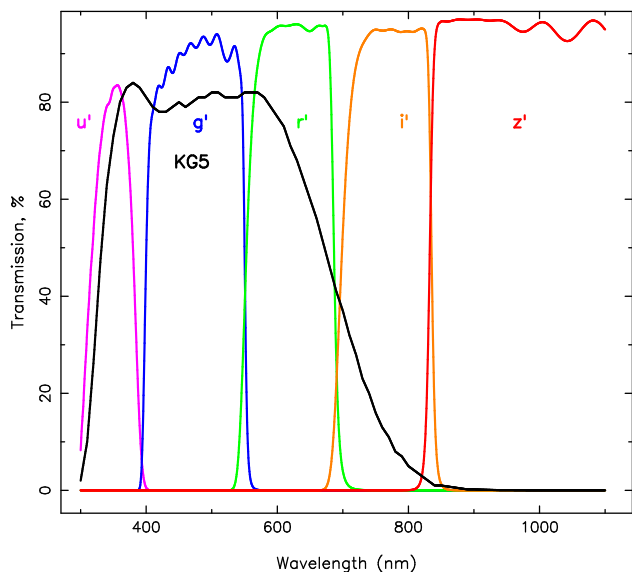
Figure A1. Transmission as a function of wavelength for the five SDSS filters and the *KG5* filter used in ultraspec.

N. V., Bikmaev I. F., Sakhibullin N. A., 2010, in American Institute of Physics Conference Series, Vol. 1273, American Institute of Physics Conference Series, Werner K., Rauch T., eds., p. 346

Yecheistov V. et al., 2014, The Astronomer's Telegram, 6300, 1

Zacharias N., Monet D. G., Levine S. E., Urban S. E., Gaume R., Wycoff G. L., 2004, in Bulletin of the American Astronomical Society, Vol. 36, American Astronomical Society Meeting Abstracts, p. 1418

Zengin Çamurdan D., İbanoğlu C., Çamurdan C. M., 2010, New Astronomy, 15, 476

Zorotovic M., Schreiber M. R., Gänsicke B. T., 2011, A&A, 536, A42

APPENDIX A: CALIBRATING THE *KG5* FILTER

In Section 3 we explained that many observations made with ultraspec at the TNT were conducted with the wide-throughput *KG5* filter. The transmission of this filter and of the standard SDSS filters are shown in Figure A1.

To calibrate the fluxes of observations in the standard SDSS filters, we simply compared the observed counts of a stable well-studied photometric standard star with its catalogued magnitude. However, this approach breaks down for the *KG5* filter, because no catalogued *KG5* magnitudes exist for standard stars. Instead, we needed to produce theoretical *KG5* magnitudes for these stars.

As discussed by Bell et al. (2012), one method for calculating theoretical magnitudes in any filter is to use bolometric corrections (BCs). BCs are unique to every star, and are the difference between the magnitude of the star in a particular filter, and the bolometric (all wavelengths) magnitude of that star, such that $M_{bol} = m_g + BC_g$ for the SDSS *g*-filter for example. If we know the BC for a photometric standard star in both the SDSS *g*-filter and the ultraspec *KG5*-filter, those corrections can be used along with the SDSS catalogue *g*-band magnitude to predict the *KG5* magnitude, as shown in Equation A1:

$$m_{KG5} + BC_{KG5} = m_g + BC_g \tag{A1}$$

To calculate a BC for any given star, we need the star's spectrum and a model of our telescope, instrument and detector throughput as a function of wavelength. Example stellar spectra are available from spectral atlases (e.g. Gunn & Stryker 1983; Pickles 1998; Castelli & Kurucz 2004), and we had already produced a throughput model for ultraspec in order to quantify the performance of the instrument during commissioning (Dhillon et al. 2014). Our model for the system includes the throughput of the atmosphere, telescope mirrors, instrument lenses and adhesives, the filters themselves, and the quantum efficiency of the detector. We used the most accurate available transmission data, with the largest uncertainties expected to come from the atmospheric extinction and the mirror reflectivity. We have no wavelength dependent information for the mirrors, or in fact any measurement of reflectivity at all, so we assumed a uniform reflectivity of 85%, repeated across all four mirrors of the TNT. We discuss the accuracy of this throughput model below in Section A1.

The formula for calculating a BC for the *g*-filter in the AB magnitude system is shown in Equation A2 and follows from the derivations in Bell et al. (2012).

$$BC_g = M_{bol\odot} - 2.5\log_{10}\left(\frac{4\pi(10pc)^2 F_{bol}}{L_\odot}\right)$$
$$+ 2.5\log_{10}\left(\frac{\int_g \lambda F_\lambda 10^{-0.4A_\lambda} R_\lambda d\lambda}{\int_g \frac{c}{\lambda} f_\nu^0 R_\lambda d\lambda}\right), \tag{A2}$$

where $F_{bol} = \sigma T_{eff}^4$ by the Stefan-Boltzmann law, F_λ is the flux at the stellar surface according to the model atmosphere spectrum, A_λ is the appropriate galactic extinction curve, and R_λ is the instrument throughput model as a function of wavelength. All functions of wavelength are handled in units of Å. We used the following values for the Sun's bolometric magnitude and the AB magnitude zero flux: $M_{bol\odot} = 4.74$ and $f_\nu^0 = 3631 \times 10^{-23}$erg s^{-1}cm^{-2}Hz^{-1}.

Since the BCs are dependent on the spectrum of the star in question, they will vary as a function of effective temperature (T_{eff}) and surface gravity (log g). Thus our final aim is to create a table of *KG5* magnitude transformations from a given *g*-band magnitude, as a function of effective temperature. This could then be used to estimate a *KG5* magnitude for any photometric standard star.

We began by creating a list of T_{eff}/log g pairs from the Dartmouth isochrone database (Dotter et al. 2008), to sample a range of effective temperatures. Since most standard stars are bright and nearby, we assumed no reddening ($E(B-V) = 0$), and solar metallicity (Fe/H = 0). Incorporating a value for the reddening into the production of the isochrone allows us to ignore the A_λ term in Equation A2.

To investigate a wider ranger of available temperatures, we sampled two age scenarios; 0.5 Gyrs (log age = 8.699) and 2 Gyrs (log age = 9.301). Since the model spectra available are generally constrained to main sequence stars, we rejected those pairs with log $g < 4$, as these values are
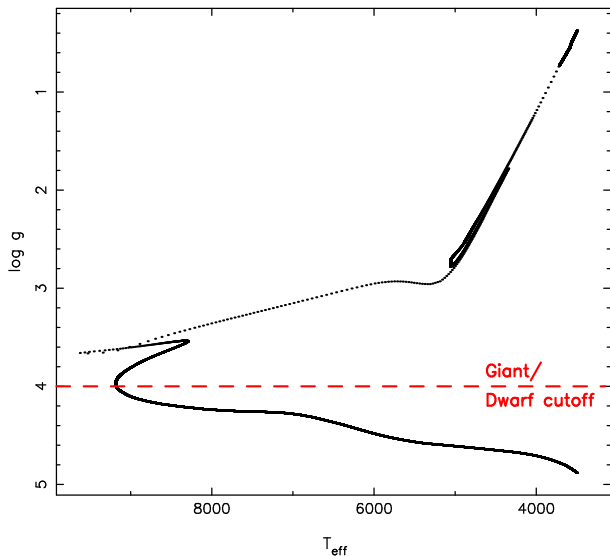
Figure A2. Theoretical T_{eff}/log g pairs for stars with no reddening, solar metallicity and an age of 0.5 Gyrs, generated from the Dartmouth isochrone database. Axes have been inverted to simulate a classical colour-magnitude diagram. We select only the main sequence stars by making a cut at log $g = 4$.

usually only found in evolved stars. This means that our final theoretical *KG5* magnitudes are only applicable to main sequence standard stars. An example isochrone of T_{eff}/log g pairs for the 0.5 Gyr scenario is shown in Figure A2.

For every theoretical star described by the Dartmouth isochrone, we generated a model spectrum using the atlas of Castelli & Kurucz (2004) and the Python module PYSYNPHOT (STScI Development Team 2013). We then calculated a *KG5* BC for every star using Equation A2, along with these model spectra and our instrument throughput model. The BCs apply to given effective temperatures, sampling the range 3500K to 9200K, in steps of a few Kelvin.

Now, supplied with the catalogue *g*-band magnitude and the effective temperature (estimated from the spectral type, within the range 3500-9200K) of any given main sequence standard star, we are able to calculate a theoretical *KG5* magnitude for that standard star using Equation A1 and linear interpolation of the existing sample. This enabled us to flux calibrate observations taken in the *KG5* filter.

A1 Accuracy of the instrumental throughput model

If we are to trust our *KG5* flux calibration procedure outlined above, we need to be sure that our throughput model for ULTRASPEC is accurate and reliable. When testing the throughput model by comparison with observations, we found that the model matched observations better in some filters than in others. This suggested that the model may be non-uniformly accurate as a function of wavelength. To investigate this, we followed the procedure of Bell et al. (2012) to calculate values of dm, the difference between theoretical and observed magnitudes in a standard filter m, as a function of SDSS colour (*g-r*), for a large selection of stars.

We obtained observations of the open cluster NGC 6940, and used these to test the throughput model accuracy. We measured observational magnitudes for stars in the cluster, and also computed theoretical magnitudes for these stars using BCs and their SDSS catalogue magnitudes. The model spectra used in the BC calculations were tailored to the properties of the cluster, being derived from a suitable isochrone; log age = 8.858, metallicity Fe/H = 0.01, E(B-V) = 2.14 (Wu et al. 2009). We used the SDSS colour versus effective temperature relation given in Equation A3 and taken from Fukugita et al. (2011) to estimate temperatures for each star in the cluster.

$$T_{eff} = \frac{1.09 \times 10^4}{1.47 + g - r} \qquad (A3)$$

We also rejected anomalous stars based on a χ^2 analysis, in which we compared the actual measured magnitudes of stars with the predicted magnitudes in a given filter, calculated using BCs and the catalogue magnitudes in the other filters. Stars with measured magnitudes more than 3-σ away from their predicted magnitudes in any filter were rejected.

We compared the predicted magnitudes produced by the BC analysis with the SDSS catalogue magnitude for each star, calculating dm as the difference between the two. Any non-uniform inaccuracy in the throughput model should be apparent as a trend of dm against the colour of the star. An example plot of dm against *g-r* is shown in Figure A3 for the ULTRASPEC g' filter. The same behaviour was seen in other filters, except in u' where the data is so sparse and scattered that we cannot conclude anything with certainty.

We found that in all filters the theoretical magnitudes matched the observed magnitudes (except for a uniform efficiency factor, likely due to the actual mirror reflectivity being different to our assumed value), with no significant trend as a function of colour. However, the available data were not sufficient to constrain this behaviour strongly, with a scatter of up to 0.2 magnitudes.

These investigations have confirmed that our throughput model is correct as a function of wavelength, and would give accurate BCs to within a systematic error of 0.2 magnitudes.

APPENDIX B: SUPPLEMENTARY ONLINE MATERIALS
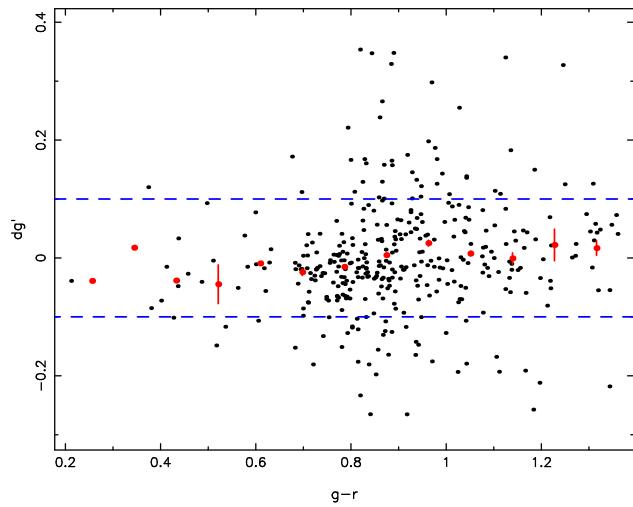
Figure A3. The difference between the theoretical and measured ULTRASPEC g'-band magnitudes of stars in NGC 6940, as a function of their colour. Individual stars are represented by black points, whilst red circles show the mean dg' of 13 equally spaced bins in colour. The error bars on the binned points are the maximum photometric uncertainty within each bin, divided by the number of points in the bin. The blue dashed lines show the ± 0.1 magnitude level with respect to zero.

Table B1: Journal of Observations. The systems are ordered alphabetically, and some system names have been shortened. Start(MJD) is the start time of each observing run, given in MJD(UTC). Mid-eclipse times are given in BMJD(TDB) and the number in parentheses is the uncertainty in the last digit. T_{exp} is the exposure time in seconds and is supplied as $T_{blue}/T_{green}/T_{red}$ for the three beams of ULTRACAM. ΔT is the duration of the observing run in minutes. Mag. is the estimated out-of-eclipse magnitude.

Object	Start (MJD)	Mid-eclipse time (BMJD)	T_{exp} (s)	ΔT (min)	Tel./Inst.	Filter	Mag.
1RXS J180834.7+101041	55316.33464	55316.3613(3) 55316.4310(3)	6/2/2	141	NTT/UCAM	$u'/g'/r'$	16.9/16.9/16.6
	55334.37156	55334.4299(3)	10/2/2	101	NTT/UCAM	$u'/g'/r'$	17.0/17.0/16.8
ASASSN-13cx	56943.91536	56943.9710(3)	150	137	pt5m	V	16.1
	56968.81315	56968.8218(3) 56968.9015(3)	150	206	pt5m	V	18.0
	56973.81141	56973.8401(7) 56973.9186(7)	150	406	pt5m	V	18.3
	56989.65725	56989.68988(3)	3.9	60	TNT/USPEC	g'	18.9
	56993.59267	-	3.9	53	TNT/USPEC	KG5	17.9
	57014.83182	57014.8596(2)	120	69	pt5m	V	16.2
	57015.86791	57015.89471(7)	120	69	pt5m	V	16.1
	57023.51317	57023.54121(3)	3.9	57	TNT/USPEC	KG5	18.5
	57024.56187	57024.57665(3)	4.9	46	TNT/USPEC	g'	18.3
	57027.56687	57027.60339(3)	5.9	69	TNT/USPEC	KG5	18.9
	57198.12288	57198.13413(15)	12/4/4	31	WHT/UCAM	$u'/g'/r'$	18.4/18.4/18.3
ASASSN-14cl	56827.07177	-	10	188	pt5m	V	11.3
	56829.08098	-	10	180	pt5m	V	11.6
	56852.08564	-	10	184	pt5m	V	16.7
ASASSN-14ds	56853.00227	-	60	304	pt5m	V	16.7
	56854.99663	-	60	314	pt5m	V	16.7
	56855.99399	-	60	318	pt5m	V	16.9
	56856.99123	-	60	183	pt5m	V	16.8
	56858.98604	-	60	310	pt5m	V	17.1
	56859.98344	-	60	170	pt5m	V	17.0
ASASSN-14gl	56995.80900	-	60	124	pt5m	V	18.2
	56998.80903	-	60	147	pt5m	V	18.6
	57016.88881	-	120	129	pt5m	V	19.1
	57018.81524	-	120	348	pt5m	V	19.3
	57016.88881	-	120	129	pt5m	V	18.2
ASASSN-14gu	57057.83442	-	120	141	pt5m	V	18.0
	57058.83810	-	120	105	pt5m	V	17.3
	57084.89539	-	120	253	pt5m	V	16.4
ASASSN-14hk	56922.12637	-	60	172	pt5m	V	15.8
	56932.99821	-	60	128	pt5m	V	17.1
ASASSN-14mv	57026.59217	-	1.0	122	TNT/USPEC	g'	11.8
ASASSN-15au	57059.83530	57059.8614(1) 57059.9302(3)	120	226	pt5m	V	18.1
	57067.00211	57067.0322(2) 57067.1011(2)	120	148	pt5m	V	18.0
	57067.89695	57067.9283(2)	120	69	pt5m	V	18.4
	57067.97227	57067.9974(3)	120	69	pt5m	V	18.1

continued from previous page.

Object	Start (MJD)	Mid-eclipse time (BMJD)	T_{exp} (s)	ΔT (min)	Tel./Inst.	Filter	Mag.
	57068.03489	57068.0665(2)	120	69	*pt5m*	V	18.1
	57076.52507	57076.54688(5)	7.0	40	TNT/USPEC	g'	18.3
	57077.62875	57077.65003(5)	7.0	39	TNT/USPEC	r'	18.5
	57106.52037	57106.54011(5)	4.0	37	TNT/USPEC	g'	18.2
	57367.70969	57367.72165(5)	10	36	TNT/USPEC	g'	17.8
ASASSN-15bu	57079.51212	57079.52541(5)	3.9	38	TNT/USPEC	g'	17.6
	57080.51411	57080.52418(5)	3.8	51	TNT/USPEC	g'	17.8
	57081.51652	57081.52293(5)	3.9	48	TNT/USPEC	g'	17.9
	57082.51514	57082.52163(5)	4.9	35	TNT/USPEC	g'	18.0
ASASSN-15ni	57231.92628	-	10	114	*pt5m*	V	13.2
	57232.90219	-	20	311	*pt5m*	V	13.6
	57235.90511	-	30	287	*pt5m*	V	14.1
	57236.89403	-	30	138	*pt5m*	V	14.2
CSS080227:112634-100210	57333.97234	55333.98693(3) 55334.06433(3)	9/3/3	154	NTT/UCAM	$u'/g'/r'$	18.6/18.7/18.4
	55711.01379	55711.03000(3)	12/4/4	41	NTT/UCAM	$u'/g'/r'$	18.3/18.5/18.1
	56046.90666	-	8.5/4.2/4.2	25	WHT/UCAM	$u'/g'/r'$	18.4/18.5/18.3
	56685.91260	56685.92246(3)	4.9	31	TNT/USPEC	$KG5$	18.3
	57076.88173	57076.90134(3)	9.9	41	TNT/USPEC	$KG5$	19.1
	57077.81348	57077.83043(3)	9.9	39	TNT/USPEC	$KG5$	19.0
	57078.80800	57078.83694(3)	9.9	56	TNT/USPEC	$KG5$	19.0
CSS080306:082655-000733	56045.86872	56045.87387(3)	6/2/2	14	WHT/UCAM	$u'/g'/r'$	20.3/19.9/20.0
	56045.90974	56045.93365(3)	12/4/4	42	WHT/UCAM	$u'/g'/r'$	20.2/20.0/19.9
	56046.86831	56046.88989(3)	12/4/4	36	WHT/UCAM	$u'/g'/r'$	19.8/19.8/19.6
	56689.94364	56689.95507(3)	3.0	26	SALT/SALTICAM	r'	19.7
	56693.87936	56693.89955(3)	3.0	39	SALT/SALTICAM	r'	20.1
	56694.95652	56694.97525(3)	3.0	33	SALT/SALTICAM	g'	20.1
	56695.96725	56695.99128(3)	3.0	44	SALT/SALTICAM	g'	20.3
	56988.76551	56988.77724(5)	5.9	31	TNT/USPEC	$KG5$	19.7
CSS080623:140454-102702	55329.21114	55329.23537(3)	13/3.3/3.3	41	NTT/UCAM	$u'/g'/r'$	19.8/19.8/19.6
	55334.09572	55334.12090(3)	15/5/5	59	NTT/UCAM	$u'/g'/r'$	20.1/19.8/19.8
	55334.15978	55334.18049(3)	16/4/4	60	NTT/UCAM	$u'/g'/r'$	20.1/19.9/19.8
	55334.20345	55334.24003(3)	12/4/4	67	NTT/UCAM	$u'/g'/r'$	20.1/19.9/19.9
	55355.01296	55355.03309(3)	7.7/3.8/3.8	41	NTT/UCAM	$u'/g'/r'$	19.7/19.7/19.5
	55355.12826	55355.15230(3)	7.7/3.8/3.8	49	NTT/UCAM	$u'/g'/r'$	20.0/19.8/19.7
	55709.03970	55709.05135(3)	6/3/3	21	NTT/UCAM	$u'/g'/r'$	19.9/19.8/19.9
	55711.95380	55711.97074(3)	12/4/4	29	NTT/UCAM	$u'/g'/r'$	19.8/19.7/19.9
	55711.99633	55712.03031(3)	12/4/4	53	NTT/UCAM	$u'/g'/r'$	20.1/19.8/19.9
	55712.11378	55712.14946(3)	12/4/4	67	NTT/UCAM	$u'/g'/r'$	20.0/19.7/19.9
CSS081220:011614+092216	56489.16741	56489.17702(3)	9.8/3.2/3.2	28	WHT/UCAM	$u'/g'/i'$	19.5/19.6/19.3
	56500.15832	56500.17282(3)	9.8/3.2/3.2	35	WHT/UCAM	$u'/g'/r'$	19.2/19.4/19.3
	56504.17318	56504.18927(3)	9.8/3.2/3.2	33	WHT/UCAM	$u'/g'/i'$	19.1/19.2/18.9
	56510.10544	56510.11505(3)	6.5/3.2/3.2	30	WHT/UCAM	$u'/g'/r'$	17.7/17.8/17.8
	56657.84860	56657.86688(3)	9.8/3.2/3.2	48	WHT/UCAM	$u'/g'/r'$	18.8/18.9/18.7
	56657.92579	56657.93272(3)	9.8/3.2/3.2	24	WHT/UCAM	$u'/g'/r'$	19.1/19.3/19.1
	56658.89473	56658.92033(3)	12/4/4	50	WHT/UCAM	$u'/g'/r'$	19.2/19.4/19.2
	56683.54083	56683.54564(3)	5.9	21	TNT/USPEC	$KG5$	19.5
	56685.57737	56685.58670(8)	9.4	33	TNT/USPEC	$KG5$	19.6
	56689.53020	56689.53730(4)	9.4	22	TNT/USPEC	$KG5$	19.2
	56873.08525	56873.10772(3)	9/3/3	57	WHT/UCAM	$u'/g'/r'$	19.0/19.0/18.8
	56874.07296	56874.09532(3)	9/3/3	41	WHT/UCAM	$u'/g'/r'$	18.8/18.9/18.8
	56988.71680	56988.72799(3)	4.1	24	TNT/USPEC	$KG5$	19.0

continued from previous page.

Object	Start (MJD)	Mid-eclipse time (BMJD)	T_{exp} (s)	ΔT (min)	Tel./Inst.	Filter	Mag.
	56989.50680	56989.51817(3)	4.1	20	TNT/USPEC	*KG5*	19.2
	57366.64759	57366.66722(3)	7.9	48	TNT/USPEC	*KG5*	16.7
CSS090102:132536+210037	55711.97933	55711.98534(2)	15/5/5	19	NTT/UCAM	$u'/g'/r'$	19.9/19.9/19.7
	55712.03626	55712.04774(2)	15/5/5	26	NTT/UCAM	$u'/g'/r'$	19.8/19.9/19.6
	55714.01658	55714.04404(2)	15/5/5	100	NTT/UCAM	$u'/g'/r'$	19.8/19.9/19.6
		55714.10641(2)					
	55943.10286	55943.12141(1)	18/6/6	50	WHT/UCAM	$u'/g'/r'$	20.4/20.2/20.1
	55943.21976	55943.24618(1)	18/6/6	55	WHT/UCAM	$u'/g'/r'$	19.9/19.8/19.8
	56873.87607	56873.90434(1)	9/3/3	57	WHT/UCAM	$u'/g'/r'$	20.2/20.1/20.2
	56874.89075	56874.90250(1)	9/3/3	31	WHT/UCAM	$u'/g'/i'$	20.1/20.1/20.2
CSS090219:044027+023301	56960.08801	-	150	50	*pt5m*	V	18.1
	56961.02405	-	150	340	*pt5m*	V	18.5
	57003.94554	-	150	54	*pt5m*	V	18.6
	57015.91831	-	150	295	*pt5m*	V	18.6
CSS090419:162620-125557	56486.92629	56486.93325(5)	12/4/4	18	WHT/UCAM	$u'/g'/i'$	21.3/21.1/20.6
	56498.90349	56498.92860(5)	12/4/4	58	WHT/UCAM	$u'/g'/i'$	20.7/20.6/20.0
	56499.87896	56499.90938(5)	12/4/4	55	WHT/UCAM	$u'/g'/r'$	20.7/20.8/20.4
	56501.92501	56501.94635(5)	15/3.9/3.9	50	WHT/UCAM	$u'/g'/i'$	20.9/20.7/20.1
	56508.87512	56508.88707(5)	12/4/4	30	WHT/UCAM	$u'/g'/r'$	20.5/20.4/20.2
	56508.95486	56508.96249(5)	12/4/4	26	WHT/UCAM	$u'/g'/r'$	21.1/21.0/20.5
	56872.87452	56872.89818(5)	4.2/4.2	51	WHT/UCAM	g'/r'	21.8/20.4
CSS090622:215636+193242	56873.91771	56873.9890(5)	120	243	*pt5m*	V	19.2
		56874.0621(5)					
	56874.10512	56874.13184(5)	9/3/3	49	WHT/UCAM	$u'/g'/r'$	19.6/19.5/19.1
	56874.19057	56874.20268(5)	9/3/3	24	WHT/UCAM	$u'/g'/r'$	19.5/19.6/19.2
	56874.96361	56874.98303(5)	9/3/3	36	WHT/UCAM	$u'/g'/i'$	19.2/19.2/18.0
	56877.93877	56877.96200(5)	9/3/3	39	WHT/UCAM	$u'/g'/i'$	20.0/19.9/18.7
	56878.15537	56878.17474(5)	9/3/3	39	WHT/UCAM	$u'/g'/i'$	19.7/19.6/18.3
	56880.20188	56880.23174(5)	9/3/3	47	WHT/UCAM	$u'/g'/i'$	19.7/19.8/18.3
	56992.49766	56992.5128(2)	5.9	37	TNT/USPEC	*KG5*	19.5
CSS091116:232551-014024	56924.94657	-	100	289	*pt5m*	V	18.9
	56939.84366	-	150	369	*pt5m*	V	18.4
CSS100218:043829+004016	56657.88694	56657.89355(2)	12/4/4	11	WHT/UCAM	$u'/g'/r'$	19.3/19.5/19.3
	56657.94634	56657.95904(1)	12/4/4	26	WHT/UCAM	$u'/g'/r'$	19.3/19.5/19.3
	56658.99048	56659.00696(1)	12/4/4	20	WHT/UCAM	$u'/g'/r'$	20.2/19.9/19.7
	56991.77750	-	6.0	53	TNT/USPEC	*KG5*	19.9
	57081.57619	-	30	50	TNT/USPEC	*KG5*	20.2
CSS100508:085604+322109	57091.85566	-	150	141	*pt5m*	V	19.5
	57097.91622	-	150	288	*pt5m*	V	19.8
CSS100520:214426+222024	56938.83073	-	120	353	*pt5m*	V	18.0
CSS110113:043112-031452	55580.09688	55580.12266(5)	7.2/2.4/2.4	47	NTT/UCAM	$u'/g'/i'$	16.1/15.8/15.9
	55940.94016	55940.95858(3)	12/4/4	37	WHT/UCAM	$u'/g'/r'$	19.9/19.9/19.5
	55942.00021	55942.01540(3)	20/5/5	32	WHT/UCAM	$u'/g'/r'$	20.1/20.0/19.7
	55942.85431	55942.87405(3)	12/4/4	34	WHT/UCAM	$u'/g'/r'$	20.0/20.0/19.8
	56180.11393	56180.12877(3)	12/4/4	30	WHT/UCAM	$u'/g'/r'$	19.7/19.8/19.6
	56214.05905	56214.07895(3)	9/3/3	35	WHT/UCAM	$u'/g'/r'$	19.8/19.8/19.6
	56659.90460	56659.92234(3)	12/4/	27	WHT/UCAM	$u'/g'/r'$	19.1/19.0/18.7
	56685.54492	56685.55006(3)	9.4	19	TNT/USPEC	*KG5*	20.0
	56685.60074	56685.61612(3)	9.4	35	TNT/USPEC	*KG5*	20.1

continued from previous page.

Object	Start (MJD)	Mid-eclipse time (BMJD)	T_{exp} (s)	ΔT (min)	Tel./Inst.	Filter	Mag.
	56686.50253	56686.54082(3)	9.4	81	TNT/USPEC	g'	19.8
	56689.56937	56689.57917(3)	9.0	44	TNT/USPEC	g'	19.8
	56730.84840	56730.86095(3)	8.0/2.6/2.6	42	WHT/UCAM	$u'/g'/r'$	19.7/19.7/19.4
CSS110114:091246-034916	57046.98180	-	120	105	pt5m	V	18.0
	57051.94906	-	120	105	pt5m	V	16.4
	57053.99243	-	120	295	pt5m	V	17.8
	57054.99178	-	120	291	pt5m	V	18.4
CSS110226:112510+231036	57049.06558	-	150	318	pt5m	V	19.5
	57068.08501	-	120	121	pt5m	V	19.5
	57070.05512	-	120	304	pt5m	V	19.7
CSS110513:210846-035031	56176.01207	56176.0486(4)	120	126	pt5m	V	17.7
	56176.91862	56176.9894(3)	120	239	pt5m	V	17.9
	56177.85543	56177.9306(3)	120	157	pt5m	V	17.9
	56486.97477	56487.0769(3)	60	209	pt5m	V	18.3
	56489.07325	56489.11534(8)	11/3.8/3.8	80	WHT/UCAM	$u'/g'/i'$	18.6/18.3/17.4
	56508.97803	56509.04487(8)	11/3.8/3.8	115	WHT/UCAM	$u'/g'/r'$	18.5/18.3/17.7
	56871.98925	56872.01611(5)	8/2/2	64	WHT/UCAM	$u'/g'/r'$	18.0/17.9/17.5
	56872.94317	56872.95764(5)	9.1/2.2/2.2	40	WHT/UCAM	$u'/g'/r'$	18.0/17.9/17.5
CSS111003:054558+022106	56976.09353	56976.1086(6)	150	61	pt5m	V	18.6
	56987.07470	-	150	135	pt5m	V	18.2
	57017.93566	57017.9642(5)	150	76	pt5m	V	18.8
	57020.91573	57020.9908(8)	150	342	pt5m	V	19.1
		57021.1107(7)					
	57024.71894	57024.7369(2)	3.9	78	TNT/USPEC	$KG5$	18.7
	57027.61787	57027.6402(2)	9.7	53	TNT/USPEC	$KG5$	18.7
	57028.93920	57028.9727(5)	120	69	pt5m	V	19.2
	57077.58668	57077.6014(2)	8.9	57	TNT/USPEC	g'	19.1
	57078.53462	57078.5690(2)	8.9	87	TNT/USPEC	r'	18.5
	57365.74728	-	15	38	TNT/USPEC	g'	19.1
	57367.68063	57367.6917(2)	16	36	TNT/USPEC	g'	19.0
CSS111019:233313-155744	55867.80455	55867.8116(6)	20/10/10	53	WHT/UCAM	$u'/g'/r'$	20.1/19.7/19.4
	56874.14164	56874.1486(1)	9/3/3	130	WHT/UCAM	$u'/g'/r'$	18.4/18.2/18.2
		56874.1914(1)					
		56874.2342(1)					
	56878.18496	56878.2193(2)	7/2.3/2.3	54	WHT/UCAM	$u'/g'/i'$	20.0/19.5/19.3
	56879.18534	56879.2049(5)	9/3/3	80	WHT/UCAM	$u'/g'/i'$	20.1/19.7/19.4
CSS111101:233003+303301	56874.09009	56874.155(1)	120	191	pt5m	V	18.1
	56874.95930	56875.092(1)	120	256	pt5m	V	18.2
	56876.95942	56877.118(1)	120	259	pt5m	V	18.1
	57016.81470	57016.8744(1)	150	104	pt5m	V	17.6
	57017.83588	-	120	140	pt5m	V	18.4
	57020.81609	-	120	140	pt5m	V	18.4
	57026.53984	57026.5459(3)	7.9	71	TNT/USPEC	$KG5$	18.5
	57026.83120	57026.8580(5)	120	69	pt5m	V	18.0
	57028.53937	57028.5731(3)	7.9	94	TNT/USPEC	$KG5$	18.4
	57028.85964	57028.8857(6)	120	69	pt5m	V	18.5
CSS130906:064726+491542	56542.20638	-	2	49	pt5m	V	13.8
	57043.96248	-	120	321	pt5m	V	17.5
CSS131106:052412+004148	56604.20805	-	35	99	pt5m	V	15.6
	56940.10939	56940.181(9)	120	204	pt5m	V	17.8

continued from previous page.

Object	Start (MJD)	Mid-eclipse time (BMJD)	T_{exp} (s)	ΔT (min)	Tel./Inst.	Filter	Mag.
	56943.14634	56943.150(9)	150	153	*pt5m*	V	18.2
	56946.10810	56946.117(1)	150	210	*pt5m*	V	15.8
	56956.18535	56956.248(9)	150	105	*pt5m*	V	18.1
	56970.03219	56970.0459(2)	150	142	*pt5m*	V	16.2
	56976.15126	56976.160(3)	150	152	*pt5m*	V	18.1
	56987.00005	-	150	104	*pt5m*	V	18.2
	56990.78805	56990.83142(5)	4.9	96	TNT/USPEC	g'	18.6
	56992.71556	56992.75265(5)	4.9	86	TNT/USPEC	$KG5$	17.9
	57023.63566	57023.66863(5)	7.9	68	TNT/USPEC	$KG5$	18.1
	57027.65700	57027.68606(5)	8.0	73	TNT/USPEC	$KG5$	18.3
	57080.59617	57080.60994(5)	15	65	TNT/USPEC	g'	18.0
	57361.78732	57361.82302(5)	5.0	95	TNT/USPEC	g'	18.0
	57365.64517	57365.666(2)	15	55	TNT/USPEC	u'	18.3
	57417.49956	57417.54151(5)	8.0	100	TNT/USPEC	g'	18.2
CSS140402:173048+554518	56754.06043	-	15	78	*pt5m*	V	14.6
CSS140901:013309+133234	56904.17086	-	170	97	*pt5m*	V	16.7
	56908.07756	-	150	233	*pt5m*	V	17.1
	56913.97688	-	150	177	*pt5m*	V	17.8
CSS141005:023428-045431	56969.93998	-	60	120	*pt5m*	V	14.6
	56995.95685	-	60	174	*pt5m*	V	14.7
	56997.88016	-	60	276	*pt5m*	V	14.9
	56998.91431	-	60	107	*pt5m*	V	14.7
	57027.88719	-	60	148	*pt5m*	V	14.8
CSS141117:030930+263804	57038.82444	-	120	51	*pt5m*	V	18.2
	57041.82943	-	120	158	*pt5m*	V	18.5
	57052.85159	-	120	48	*pt5m*	V	18.3
	57053.83222	-	120	160	*pt5m*	V	18.4
	57054.83256	-	120	225	*pt5m*	V	18.3
CzeV404 Her	56740.83024	56740.86289(8)	4.4	77	TNT/USPEC	g'	17.1
	56742.88593	56742.9211(2)	3.4	82	TNT/USPEC	g'	15.1
	56854.02607	56854.0773(2)	60	98	*pt5m*	V	14.8
	56856.89675	56856.9201(2)	60	69	*pt5m*	V	14.1
	56871.87078	56871.91729(5)	3.6/1.8/1.8	80	WHT/UCAM	$u'/g'/r'$	17.1/17.0/16.6
	57079.90232	57079.91840(5)	3.4	58	TNT/USPEC	$KG5$	16.1
	57083.92911	57083.9373(2)	3.4	33	TNT/USPEC	$KG5$	14.9
Gaia15aan	57054.25900	-	30	40	*pt5m*	V	18.3
	57055.25668	-	30	42	*pt5m*	V	18.6
	57057.21084	-	60	107	*pt5m*	V	18.6
	57059.17340	-	60	40	*pt5m*	V	18.8
GALEX J003535.7+462353	55940.81525	55940.8250(1)	5.6/1.8/1.8	50	WHT/UCAM	$u'/g'/r'$	17.1/17.0/16.6
	55941.83001	55941.8592(5)	5.6/1.8/1.8	65	WHT/UCAM	$u'/g'/r'$	16.5/15.9/15.7
	56179.91441	56179.9424(1)	4.6/1.5/1.5	65	WHT/UCAM	$u'/g'/r'$	16.7/16.4/16.1
	56209.90088	56209.9185(1)	6/2/2	55	WHT/UCAM	$u'/g'/r'$	16.4/16.3/15.9
	56210.93470	56210.9523(1)	5/1/1	39	WHT/UCAM	$u'/g'/r'$	16.6/16.3/16.1
	56500.18602	56500.2015(1)	6/2/2	78	WHT/UCAM	$u'/g'/r'$	16.4/16.3/16.0
	56505.17727	56505.1977(1)	6/2/2	53	WHT/UCAM	$u'/g'/i'$	17.0/16.9/16.3
	56509.99699	56510.0215(1)	6/2/2	75	WHT/UCAM	$u'/g'/r'$	16.9/16.8/16.4
	56510.16914	56510.1936(1)	6/2/2	65	WHT/UCAM	$u'/g'/r'$	16.7/16.5/16.2
	56657.79859	56657.8333(1)	6/2/2	68	WHT/UCAM	$u'/g'/r'$	16.6/16.3/16.0
	56658.83889	56658.8669(1)	6/2/2	75	WHT/UCAM	$u'/g'/r'$	16.4/16.4/15.9
	56872.09341	56872.1433(1)	6/2/2	100	WHT/UCAM	$u'/g'/r'$	16.6/16.4/16.1

continued from previous page.

Object	Start (MJD)	Mid-eclipse time (BMJD)	T_{exp} (s)	ΔT (min)	Tel./Inst.	Filter	Mag.
	56873.12930	56873.1770(1)	6/2/2	117	WHT/UCAM	$u'/g'/r'$	16.6/16.4/16.0
	56988.57231	56988.6012(1)	1.9	87	TNT/USPEC	$KG5$	16.4
	57023.55486	57023.5727(1)	1.9	45	TNT/USPEC	$KG5$	16.4
	57365.69822	57365.7111(1)	10	56	TNT/USPEC	g'	17.2
GY Cnc	55938.24332	55938.26366(4)	12/4/4	56	WHT/UCAM	$u'/g'/r'$	16.7/16.6/16.2
	55941.22656	55941.24626(4)	6.2/3.1/3.1	52	WHT/UCAM	$u'/g'/r'$	16.7/16.8/16.2
	55942.98285	55943.00068(4)	7.5/2.5/2.5	46	WHT/UCAM	$u'/g'/r'$	17.0/16.9/16.3
	55943.14044	55943.17605(4)	7.5/2.5/2.5	71	WHT/UCAM	$u'/g'/r'$	16.7/16.5/16.1
	55947.18590	55947.21130(4)	12/4/4	51	WHT/UCAM	$u'/g'/r'$	16.6/16.6/16.1
	56657.18967	56657.22682(5)	12/4/4	74	WHT/UCAM	$u'/g'/r'$	16.3/16.4/16.0
	56683.69249	56683.71865(5)	1.3	53	TNT/USPEC	$KG5$	16.5
	57080.55294	57080.56902(5)	2.5	50	TNT/USPEC	$KG5$	16.7
	57367.73864	57367.76812(5)	4.0	91	TNT/USPEC	$KG5$	16.6
HS 2325+8205	55941.87952	55941.89303(5)	5.6/1.8/1.8	48	WHT/UCAM	$u'/g'/r'$	14.7/14.4/14.4
	56487.16448	56487.19622(5)	5.6/1.8/1.8	94	WHT/UCAM	$u'/g'/i'$	17.1/16.7/16.1
	56509.13073	56509.15629(5)	5.6/1.8/1.8	76	WHT/UCAM	$u'/g'/r'$	15.2/14.9/14.8
HT Cas	54400.23091	54400.24274(5)	9.4/2.3/2.3	23	WHT/UCAM	$u'/g'/r'$	16.4/16.6/16.5
	56872.19923	56872.21011(5)	6.6/2.2/2.2	46	WHT/UCAM	$u'/g'/r'$	16.5/16.6/16.4
	56874.03047	56874.05133(5)	6.3/2.1/2.1	56	WHT/UCAM	$u'/g'/r'$	16.2/16.5/16.3
	56988.48215	56988.49911(5)	1.0	36	TNT/USPEC	g'	16.8
	56993.48629	56993.50711(5)	2.0	32	TNT/USPEC	g'	16.5
	57023.61271	57023.62882(5)	2.0	29	TNT/USPEC	$KG5$	16.8
	57024.65162	57024.65988(5)	2.0	22	TNT/USPEC	g'	16.7
	57285.06842	57285.07646(5)	6.6/2.2/2.2	15	WHT/UCAM	$u'/g'/r'$	16.0/16.3/16.1
IY UMa	56746.62944	56746.64028(2)	2.2	46	TNT/USPEC	$KG5$	17.6
	56746.70652	56746.71419(2)	2.2	28	TNT/USPEC	$KG5$	17.7
	56746.78005	56746.78810(2)	2.2	33	TNT/USPEC	$KG5$	17.6
	56991.93503	56991.94411(5)	3.4	28	TNT/USPEC	$KG5$	14.5
	57025.92282	57025.94209(3)	3.4	40	TNT/USPEC	g'	17.4
	57028.88243	57028.89840(5)	4.0	30	TNT/USPEC	r'	17.3
	57076.85098	57076.86533(3)	3.9	41	TNT/USPEC	r'	17.2
MAST003059.39+301634.3	56904.95602	56904.9976(3)	90	407	pt5m	V	19.4
		56905.0685(3)					
		56905.1396(5)					
		56905.2084(5)					
	56907.94797	-	120	117	pt5m	V	19.7
	56921.95125	56922.002(1)	120	148	pt5m	V	19.7
	56922.95876	56922.984(1)	120	343	pt5m	V	19.8
		56923.0559(9)					
		56923.1263(3)					
		56923.1965(8)					
	56992.64865	56992.6851(1)	5.9	61	TNT/USPEC	$KG5$	19.9
	57023.58867	57023.6008(1)	6.9	33	TNT/USPEC	$KG5$	19.2
	57199.17958	57199.18681(4)	10.5/3.5/3.5	29	WHT/UCAM	$u'/g'/r'$	19.6/19.7/19.5
	57284.89172	57284.90695(8)	20/6.7/6.7	28	WHT/UCAM	$u'/g'/r'$	19.5/19.5/19.3
MAST034045.31+471632.2	56936.97202	-	120	402	pt5m	V	18.7
MAST041923.57+653004.3	56944.02661	-	120	326	pt5m	V	17.2
	56960.12942	-	120	132	pt5m	V	17.3
	56967.11017	-	120	129	pt5m	V	17.4
MAST171921.40+640309.8	56732.06257	-	30	100	pt5m	V	16.2

continued from previous page.

Object	Start (MJD)	Mid-eclipse time (BMJD)	T_{exp} (s)	ΔT (min)	Tel./Inst.	Filter	Mag.
	56735.02752	-	40	155	*pt5m*	*V*	16.6
MAST192328.22+612413.5	56774.04124	56774.148(5)	120	263	*pt5m*	*V*	19.3
	56779.11794	56779.1753(2)	35/7/7	164	WHT/UCAM	*u′/g′/r′*	18.2/17.9/17.7
	56799.97068	-	180	176	*pt5m*	*V*	17.4
	56825.92616	56825.9488(3)	180	80	*pt5m*	*V*	18.8
	56826.92700	56826.9551(3)	180	119	*pt5m*	*V*	18.9
	56834.92790	56835.0026(3)	180	398	*pt5m*	*V*	17.2
		56835.1704(3)					
	56873.03328	56873.05815(5)	13/3.3/3.3	69	WHT/UCAM	*u′/g′/r′*	19.3/19.1/18.8
MAST194955.17+455349.6	56874.88619	-	90	106	*pt5m*	*V*	18.6
	56878.95944	-	90	292	*pt5m*	*V*	18.7
MAST201121.95+565531.1	56836.00727	-	60	203	*pt5m*	*V*	17.2
MAST202157.69+212919.4	56894.91143	-	120	304	*pt5m*	*V*	20.3
MAST203421.90+120656.9	56849.02716	-	100	264	*pt5m*	*V*	17.9
	56849.96328	-	100	262	*pt5m*	*V*	17.8
MAST210316.39+314913.6	56858.03866	-	80	255	*pt5m*	*V*	18.0
	56879.88002	-	80	425	*pt5m*	*V*	18.3
MAST232100.42+494614.0	56799.13236	56799.152(9)	60	111	*pt5m*	*V*	18.9
	56854.16419	-	90	61	*pt5m*	*V*	18.7
	56878.02050	56878.1546(4)	100	295	*pt5m*	*V*	16.9
	56880.96494	56881.128(9)	100	377	*pt5m*	*V*	18.5
	56881.99945	56882.191(6)	100	329	*pt5m*	*V*	18.7
	56884.95665	56885.160(9)	150	392	*pt5m*	*V*	18.8
	56895.12463	56895.143(4)	150	157	*pt5m*	*V*	19.0
	56921.88054	56921.902(9)	150	99	*pt5m*	*V*	19.0
	56922.05619	56922.124(9)	150	98	*pt5m*	*V*	18.7
	56943.07065	56943.136(3)	150	105	*pt5m*	*V*	18.9
	56956.03000	56956.0949(3)	150	105	*pt5m*	*V*	16.8
	56988.63813	-	4.0	87	TNT/USPEC	*KG5*	17.9
	56992.57897	56992.6242(1)	5.0	97	TNT/USPEC	*g′*	19.3
	57025.50124	57025.5411(1)	6.0	96	TNT/USPEC	*KG5*	19.0
	57028.49920	57028.5144(1)	8.0	55	TNT/USPEC	*KG5*	19.1
	57366.60377	-	14	56	TNT/USPEC	*g′*	18.5
MLS101226:072033+172437	56770.86964	56770.9453(8)	120	132	*pt5m*	*V*	18.0
	56772.87068	56772.9016(8)	120	156	*pt5m*	*V*	18.0
	57045.01865	57045.1377(6)	120	232	*pt5m*	*V*	18.3
	57048.84401	57048.897(5)	120	69	*pt5m*	*V*	18.3
	57049.01683	57049.0479(6)	120	67	*pt5m*	*V*	18.4
	57051.87424	57051.9049(4)	120	69	*pt5m*	*V*	18.6
	57056.83720	57056.8694(7)	120	69	*pt5m*	*V*	18.4
	57056.98798	57057.0204(4)	120	69	*pt5m*	*V*	18.4
	57079.71591	57079.7303(2)	6.9	52	TNT/USPEC	*g′*	18.7
MLS120517:152507-032655	56772.03312	-	180	92	*pt5m*	*V*	16.3
	56772.98238	56773.0340(5)	120	343	*pt5m*	*V*	16.5
		56773.0981(5)					
		56773.1630(5)					
	56775.95890	56775.9956(5)	120	308	*pt5m*	*V*	16.5
		56776.0600(5)					
		56776.1244(4)					

continued from previous page.

| Object	Start (MJD)	Mid-eclipse time (BMJD)	T_{exp} (s)	ΔT (min)	Tel./Inst.	Filter	Mag.
	56864.90455	56864.9069(5) 56864.9710(3)	120	104	*pt5m*	V	17.0
	56874.87061	56874.8857(3)	3.6/1.7/1.7	25	WHT/UCAM	$u'/g'/i'$	18.0/17.4/16.3
SDSS J040714.78-064425.1	54392.19660	-	10/2.5/2.5	109	WHT/UCAM	$u'/g'/r'$	17.8/17.7/17.3
	54396.19804	54396.23455(8)	20/5/5	98	WHT/UCAM	$u'/g'/r'$	17.3/17.0/16.7
	55939.82002	55939.9837(4)	10	281	*pt5m*	R	15.7
	56215.00769	56215.03344(8)	2.8/1.4/1.4	78	WHT/UCAM	$u'/g'/r'$	16.0/15.8/15.7
	57026.70536	57026.7366(2)	6.9	75	TNT/USPEC	$KG5$	15.6
	57082.54167	57082.5629(1)	6.9	74	TNT/USPEC	$KG5$	18.4
	57083.56625	57083.5841(1)	6.9	64	TNT/USPEC	$KG5$	17.8
	57367.63138	57367.6551(2)	5.1	64	TNT/USPEC	g'	15.6
SDSS J075059.97+141150.1	55940.89611	55940.92964(4)	12/4/4	58	WHT/UCAM	$u'/g'/r'$	18.9/19.1/18.9
	55940.99589	55941.02271(4)	12/4/4	66	WHT/UCAM	$u'/g'/r'$	19.2/19.3/19.1
	55942.12618	55942.14077(4)	12/4/4	41	WHT/UCAM	$u'/g'/r'$	19.3/19.6/16.4
	55943.05921	55943.07241(4)	12/4/4	30	WHT/UCAM	$u'/g'/r'$	19.3/19.7/19.5
	56211.19435	56211.20263(5)	9/3/3	29	WHT/UCAM	$u'/g'/r'$	19.1/19.4/19.3
	56657.98984	56658.02444(4)	12/4/4	69	WHT/UCAM	$u'/g'/r'$	18.9/19.2/19.0
	56658.93310	56658.95609(4)	12/4/4	39	WHT/UCAM	$u'/g'/r'$	18.8/19.0/18.8
	56659.02043	56659.04924(4)	12/4/4	47	WHT/UCAM	$u'/g'/r'$	18.8/19.0/18.8
	56683.62169	56683.64491(4)	10	45	TNT/USPEC	$KG5$	18.7
	56684.64142	56684.66967(5)	7.0	53	TNT/USPEC	$KG5$	18.4
SDSS J090103.93+480911.1	53803.84353	53803.90711(2)	5/5/5	114	WHT/UCAM	$u'/g'/r'$	19.5/19.7/19.5
	53804.98276	53804.99742(2)	5/5/5	25	WHT/UCAM	$u'/g'/r'$	19.2/19.4/19.2
	53805.12890	53805.15321(2)	5/5/5	49	WHT/UCAM	$u'/g'/r'$	19.1/19.3/19.1
	55203.93743	55203.96531(5)	6.8/1.7/1.7	48	WHT/UCAM	$u'/g'/r'$	19.4/19.6/19.5
	55942.08419	55942.11712(2)	13/4.5/4.5	56	WHT/UCAM	$u'/g'/r'$	20.0/20.0/19.8
	55942.15686	55942.19500(2)	13/4.5/4.5	74	WHT/UCAM	$u'/g'/r'$	20.2/20.2/20.0
	55942.95787	55942.97383(2)	13/4.5/4.5	31	WHT/UCAM	$u'/g'/r'$	19.5/19.6/19.5
	55943.01684	55943.05169(2)	13/4.5/4.5	56	WHT/UCAM	$u'/g'/r'$	19.7/19.8/19.6
	55943.19203	55943.20746(2)	13/4.5/4.5	34	WHT/UCAM	$u'/g'/r'$	19.5/19.6/19.5
	55943.26137	55943.28535(2)	13/4.5/4.5	51	WHT/UCAM	$u'/g'/r'$	19.7/19.7/19.5
SDSS J090403.49+035501.2	56045.88320	56045.89912(2)	12/12/12	26	WHT/UCAM	$u'/g'/r'$	19.6/19.3/19.3
SDSS J092009.54+004245.0	55700.02192	55700.10597(5)	8.7/2.9/2.9	154	NTT/UCAM	$u'/g'/r'$	17.7/18.0/17.7
	55708.95938	55708.97858(5)	5.6/2.8/2.8	57	NTT/UCAM	$u'/g'/r'$	18.2/18.0/17.7
	57026.77655	57026.84657(5)	5.9	118	TNT/USPEC	$KG5$	17.9
SDSS J092444.48+080150.9	55709.00465	55709.02440(7)	15/5/5	42	NTT/UCAM	$u'/g'/r'$	20.0/20.1/19.2
SDSS J093537.46+161950.8	55710.94728	55710.98340(6)	15/5/5	88	NTT/UCAM	$u'/g'/r'$	19.5/19.2/18.7
SDSS J100658.40+233724.4	55942.02575	55942.0530(1)	12/4/4	79	WHT/UCAM	$u'/g'/r'$	18.4/18.5/17.9
	56682.70289	56682.7302(2)	3.4	65	TNT/USPEC	$KG5$	18.2
	56682.87478	56682.9163(2)	3.4	85	TNT/USPEC	$KG5$	18.2
	56683.81609	56683.8457(2)	3.4	75	TNT/USPEC	$KG5$	18.2
	56685.85274	56685.8907(2)	3.4	81	TNT/USPEC	$KG5$	18.1
	56690.66858	56690.7244(2)	5.9	118	TNT/USPEC	g'	18.5
	56690.87758	56690.9103(2)	3.4	70	TNT/USPEC	r'	18.6
	57362.77084	57362.8006(2)	4.9	75	TNT/USPEC	g'	18.6
SDSS J115207.00+404947.8	56730.88610	56730.90933(1)	12/4/4	45	WHT/UCAM	$u'/g'/r'$	19.6/19.5/19.5
	56746.66410	56746.69503(1)	5.4	57	TNT/USPEC	$KG5$	19.7
	56746.73621	56746.76277(1)	5.4	57	TNT/USPEC	$KG5$	19.4
	56746.80606	56746.83053(1)	5.4	56	TNT/USPEC	$KG5$	19.5

continued from previous page.

Object	Start (MJD)	Mid-eclipse time (BMJD)	T_{exp} (s)	ΔT (min)	Tel./Inst.	Filter	Mag.
SDSS J125023.84+665525.4	53798.98823	53799.00334(4)	4/4/4	32	WHT/UCAM	$u'/g'/r'$	18.2/18.3/18.1
	53799.22336	53799.23838(4)	4/4/4	23	WHT/UCAM	$u'/g'/r'$	18.3/18.4/18.2
	53799.93218	53799.94313(4)	4/4/4	23	WHT/UCAM	$u'/g'/r'$	18.6/18.6/18.5
	53802.92144	53802.93866(4)	4/4/4	37	WHT/UCAM	$u'/g'/r'$	18.6/18.7/18.6
	53802.97429	53802.99743(4)	4/4/4	40	WHT/UCAM	$u'/g'/r'$	18.5/18.7/18.5
	53803.10330	53803.11493(4)	4/4/4	23	WHT/UCAM	$u'/g'/r'$	18.6/18.8/18.7
	53803.15397	53803.17368(4)	3/3/3	41	WHT/UCAM	$u'/g'/r'$	18.6/18.7/18.6
	53803.21193	53803.23237(4)	4/4/4	37	WHT/UCAM	$u'/g'/r'$	18.6/18.9/18.6
	55202.24092	55202.25763(4)	9/2.2/2.2	61	WHT/UCAM	$u'/g'/z'$	18.6/19.0/18.7
	55204.10992	55204.13721(4)	11/3.8/3.8	52	WHT/UCAM	$u'/g'/r'$	18.4/18.7/18.5
	55204.17561	55204.19589(4)	11/3.8/3.8	33	WHT/UCAM	$u'/g'/r'$	18.5/18.8/18.6
	55204.24567	55204.25463(4)	11/3.8/3.8	22	WHT/UCAM	$u'/g'/r'$	18.6/18.9/18.8
	57076.91313	57076.92429(4)	9.9	32	TNT/USPEC	*KG5*	17.9
	57077.78863	57077.80532(4)	9.9	32	TNT/USPEC	*KG5*	18.0
SDSS J152419.33+220920.1	55709.06004	55709.09910(3)	20/5/5	80	NTT/UCAM	$u'/g'/r'$	19.3/19.3/18.9
	55709.14436	55709.16439(3)	20/5/5	35	NTT/UCAM	$u'/g'/r'$	19.3/19.2/18.9
	55712.08247	55712.10372(3)	12/3/3	39	NTT/UCAM	$u'/g'/r'$	19.2/19.2/18.9
	55714.11519	55714.12865(3)	12/3/3	26	NTT/UCAM	$u'/g'/r'$	19.0/19.1/18.8
	56046.05227	56046.07845(1)	12/4/4	51	WHT/UCAM	$u'/g'/r'$	18.8/19.1/19.0
	56046.12728	56046.14374(1)	12/4/4	28	WHT/UCAM	$u'/g'/r'$	18.6/18.9/18.7
	56046.95909	56046.99289(1)	12/4/4	58	WHT/UCAM	$u'/g'/r'$	18.5/18.9/18.6
	56486.89370	56486.91454(1)	10.6/3.5/3.5	39	WHT/UCAM	$u'/g'/i'$	19.1/19.3/18.8
	56494.86606	56494.88342(1)	10.6/3.5/3.5	40	WHT/UCAM	$u'/g'/i'$	19.3/19.3/19.0
	56503.87498	56503.89742(1)	13.6/4.5/4.5	49	WHT/UCAM	$u'/g'/i'$	19.3/19.4/19.1
	56509.95159	56509.97206(1)	10.6/3.5/3.5	60	WHT/UCAM	$u'/g'/r'$	19.2/19.5/19.1
	56719.23748	56719.25331(4)	12/4/4	37	WHT/UCAM	$u'/g'/r'$	19.5/19.7/19.6
	56746.87519	56746.88311(3)	3.4	23	TNT/USPEC	*KG5*	19.4
	56871.95572	56871.96849(4)	8/2/2	43	WHT/UCAM	$u'/g'/r'$	19.0/19.2/18.9
	56873.91985	56873.92807(4)	9/2.2/2.2	24	WHT/UCAM	$u'/g'/r'$	19.0/19.2/18.8
SDSS J155531.99-001055.0	54260.20835	54260.22695(1)	6/2/2	25	VLT/UCAM	$u'/g'/r'$	19.1/19.4/19.2
	54260.27914	54260.30580(1)	6/2/2	54	VLT/UCAM	$u'/g'/r'$	19.0/19.4/19.2
	54272.98205	54272.99993(1)	6/2/2	27	VLT/UCAM	$u'/g'/r'$	19.0/19.2/19.0
	55334.26865	55334.33987(2)	15/5/5	123	NTT/UCAM	$u'/g'/r'$	19.0/19.3/19.0
	55712.20386	55712.24662(2)	11/3.5/3.5	71	NTT/UCAM	$u'/g'/r'$	19.0/19.4/19.2
	56046.21549	56046.23642(2)	12/4/4	27	WHT/UCAM	$u'/g'/r'$	19.0/19.3/19.0
	56176.86930	56176.88349(2)	14/3.5/3.5	40	WHT/UCAM	$u'/g'/r'$	19.0/19.4/19.2
	56489.01055	56489.03300(2)	9/3/3	45	WHT/UCAM	$u'/g'/i'$	19.0/19.3/19.0
	56498.88028	56498.88873(2)	9.8/3.2/3.2	23	WHT/UCAM	$u'/g'/i'$	19.1/19.4/19.1
	56501.87310	56501.88484(2)	9/3/3	24	WHT/UCAM	$u'/g'/i'$	18.9/19.3/18.9
	56872.91245	56872.93200(2)	9.8/3.2/3.2	35	WHT/UCAM	$u'/g'/r'$	18.8/19.2/18.9
	56873.93949	56873.95698(2)	9.8/3.2/3.2	48	WHT/UCAM	$u'/g'/r'$	19.0/19.2/18.9
	57081.86284	57081.87272(2)	15	32	TNT/USPEC	*KG5*	19.6
	57198.07630	57198.09102(2)	9/3/3	24	WHT/UCAM	$u'/g'/r'$	18.8/19.1/18.8
SDSS J155656.92+352336.6	54683.88334	54683.95644(4)	3.4/3.4/3.4	121	WHT/UCAM	$u'/g'/r'$	17.5/17.2/17.2
	55942.22648	55942.25538(4)	12/4/4	63	WHT/UCAM	$u'/g'/r'$	17.7/17.4/17.4
	56046.01331	56046.02708(8)	12/4/4	34	WHT/UCAM	$u'/g'/r'$	18.9/18.8/18.7
	56046.09093	56046.11505(8)	12/4/4	49	WHT/UCAM	$u'/g'/r'$	18.9/18.7/18.6
	56046.18489	56046.20324(8)	12/4/4	41	WHT/UCAM	$u'/g'/r'$	18.9/18.8/18.8
	56499.92019	-	12/4/4	51	WHT/UCAM	$u'/g'/r'$	19.1/19.1/19.0
	56501.89201	56501.9004(3) 56501.9885(3)	120	156	*pt5m*	V	18.9
	56873.97532	56873.9990(1)	6.5/2.1/2.1	46	WHT/UCAM	$u'/g'/r'$	19.0/18.8/18.8
	57079.85619	57079.8685(1)	8.9	39	TNT/USPEC	*KG5*	18.8

continued from previous page.

Object	Start (MJD)	Mid-eclipse time (BMJD)	T_{exp} (s)	ΔT (min)	Tel./Inst.	Filter	Mag.
SSS100615:200331-284941	56872.97323	56873.024417(5)	12/3/3	78	WHT/UCAM	$u'/g'/r'$	19.9/19.7/19.6
	56874.01104	56874.022391(5)	9/3/3	21	WHT/UCAM	$u'/g'/r'$	19.7/19.6/19.4
	56874.94861	56874.961664(5)	15/5/5	18	WHT/UCAM	$u'/g'/i'$	19.4/19.5/19.8
SSS120402:134015350512	57027.91986	57027.95944(5)	6.9	71	TNT/USPEC	$KG5$	18.6
SSS130413:094551-194402	56683.65823	56683.67469(5)	5.8	35	TNT/USPEC	$KG5$	17.0
	56683.72993	56683.74054(5)	5.8	21	TNT/USPEC	$KG5$	17.1
	56683.78617	56683.80628(5)	5.8	40	TNT/USPEC	$KG5$	17.0
	56684.68236	56684.72712(5)	5.8	90	TNT/USPEC	$KG5$	17.1
	56685.69475	56685.71357(5)	2.9	37	TNT/USPEC	$KG5$	17.1
	56689.63539	56689.65982(5)	2.9	46	TNT/USPEC	$KG5$	17.1
	56689.84202	56689.85708(5)	2.9	31	TNT/USPEC	$KG5$	17.1
	56690.75257	56690.77779(5)	2.9	49	TNT/USPEC	g'	17.1
	56690.82365	56690.84355(5)	2.9	33	TNT/USPEC	r'	17.0
	56699.05164	56699.06472(3)	1.0	25	SALT/SALTICAM	g'	17.0
	56739.62758	56739.6449(1)	2.9	31	TNT/USPEC	$KG5$	17.2
	56777.84234	56777.85636(3)	1.0	35	SALT/SALTICAM	g'	17.0
	57023.75635	57023.76773(3)	2.9	29	TNT/USPEC	i'	16.8
	57416.70864	57416.73923(5)	9.3	52	TNT/USPEC	u'	16.9
	57418.69218	57418.71238(5)	8.1	29	TNT/USPEC	u'	16.6
V2051 Oph	54261.28607	54261.31011(3)	1/1/1	45	VLT/UCAM	$u'/g'/r'$	15.5/15.6/15.4
	54264.16307	54264.18181(3)	1/1/1	30	VLT/UCAM	$u'/g'/r'$	15.6/15.6/15.5
	54268.27875	54268.30206(3)	3/1/1	41	VLT/UCAM	$u'/g'/r'$	15.8/15.9/15.7
	54268.34368	54268.36449(3)	3/1/1	46	VLT/UCAM	$u'/g'/r'$	16.0/16.0/15.9
	55314.14160	55314.15612(3) 55314.21854(3)	6/2/2	128	NTT/UCAM	$u'/g'/r'$	15.5/15.4/15.1
	55314.30287	55314.34340(3)	6/2/2	86	NTT/UCAM	$u'/g'/r'$	15.7/15.5/15.4
	55315.38811	55315.40460(3)	6/2/2	59	NTT/UCAM	$u'/g'/r'$	15.7/15.6/15.4
	55329.30344	55329.32629(3)	3/1.5/1.5	55	NTT/UCAM	$u'/g'/r'$	15.2/15.0/14.8
	55353.32613	55353.36077(3)	4/1.3/1.3	69	NTT/UCAM	$u'/g'/r'$	15.6/15.5/15.3
	55354.01710	55354.04752(3)	4/1.3/1.3	57	NTT/UCAM	$u'/g'/r'$	15.8/15.7/15.5
	55700.37290	55700.39738(3)	9/3/3	44	NTT/UCAM	$u'/g'/r'$	16.0/15.7/15.5
	55701.32116	55701.33373(3)	9/3/3	26	NTT/UCAM	$u'/g'/r'$	15.8/15.7/15.5
	55701.38384	55701.39615(3)	9/3/3	57	NTT/UCAM	$u'/g'/r'$	15.5/15.5/15.3
	55705.28872	55705.32906(3)	9/3/3	77	NTT/UCAM	$u'/g'/r'$	15.7/15.6/15.4
	55706.29035	55706.32798(3)	10/3.3/3.3	91	NTT/UCAM	$u'/g'/r'$	16.0/15.9/15.6
	55709.31110	55709.32452(3) 55709.38697(3)	6/2/2	95	NTT/UCAM	$u'/g'/r'$	16.0/15.8/15.6
	55710.23956	55710.26091(3)	10/2/2	34	NTT/UCAM	$u'/g'/r'$	15.7/15.5/15.4
	55713.23903	55713.25747(3)	9/3/3	34	NTT/UCAM	$u'/g'/r'$	15.8/15.8/15.6
	55713.30486	55713.31989(3)	6/2/2	31	NTT/UCAM	$u'/g'/r'$	15.8/15.7/15.5
	55713.36174	55713.38235(3)	7.4/2.4/2.4	40	NTT/UCAM	$u'/g'/r'$	15.7/15.7/15.5
	55714.24128	55714.25632(3)	8.4/2.8/2.8	64	NTT/UCAM	$u'/g'/r'$	15.8/15.6/15.5
	57080.91855	57080.92712(3)	1.9	29	TNT/USPEC	$KG5$	15.6
	57082.91711	57082.92489(3)	2.0	37	TNT/USPEC	$KG5$	15.6
	57084.91585	57084.92251(3)	2.0	22	TNT/USPEC	$KG5$	15.6
V713 Cep	55801.14595	55801.18114(2)	4.4/2.2/2.2	64	WHT/UCAM	$u'/g'/i'$	18.9/18.8/18.7
	56046.15044	-	6.3/2.1/2.1	46	WHT/UCAM	$u'/g'/r'$	18.7/18.6/18.5
	56176.90266	56176.93715(2)	10/3.4/3.4	61	WHT/UCAM	$u'/g'/r'$	18.4/18.3/18.2
	56177.84463	56177.87676(2)	10/3.4/3.4	65	WHT/UCAM	$u'/g'/r'$	18.3/18.2/18.1
	56179.99153	56180.01222(2)	10/3.4/3.4	47	WHT/UCAM	$u'/g'/r'$	18.3/18.3/18.2
	56488.17430	56488.20223(2)	10/3.4/3.4	74	WHT/UCAM	$u'/g'/z'$	18.6/18.5/17.6
	56489.04428	56489.05642(2)	10/3.4/3.4	35	WHT/UCAM	$u'/g'/i'$	18.6/18.4/18.2
	56489.13138	56489.14184(2)	10/3.4/3.4	26	WHT/UCAM	$u'/g'/i'$	18.6/18.5/18.3
	56489.18909	56489.22726(2)	10/3.4/3.4	66	WHT/UCAM	$u'/g'/i'$	18.7/18.5/18.3

Object	Start (MJD)	Mid-eclipse time (BMJD)	T_{exp} (s)	ΔT (min)	Tel./Inst.	Filter	Mag.
	56499.19598	56499.22121(2)	10/3.4/3.4	59	WHT/UCAM	$u'/g'/z'$	18.4/18.4/17.6
	56509.18559	56509.21517(2)	10/3.4/3.4	77	WHT/UCAM	$u'/g'/r'$	18.5/18.5/18.4
	56510.12816	56510.15480(2)	10/3.4/3.4	56	WHT/UCAM	$u'/g'/r'$	18.6/18.5/18.4
	56872.03795	56872.07302(3)	6/2/2	74	WHT/UCAM	$u'/g'/r'$	18.2/18.2/18.0
	56880.16994	56880.18780(3)	10/3.4/3.4	41	WHT/UCAM	$u'/g'/i'$	18.5/18.4/18.2
	57198.09643	57198.11544(2)	10/3.4/3.4	35	WHT/UCAM	$u'/g'/r'$	19.2/19.0/19.0
	57282.84397	57282.85057(2)	15/5/5	20	WHT/UCAM	$u'/g'/r'$	18.5/18.6/18.4
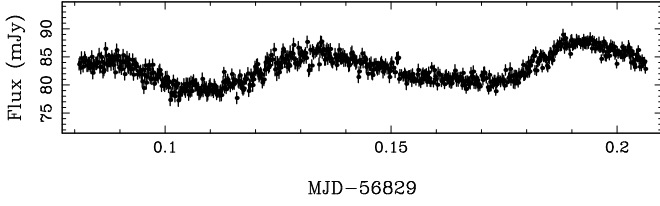
Figure B1. ASASSN-14cl light curve observed on 2014-06-20 with *pt5m*, showing superhumps with a period of approximately 1.4 hours.
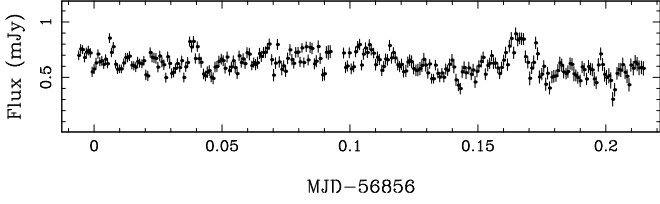
Figure B2. ASASSN-14ds light curve observed during outburst on 2014-07-17 with *pt5m*. There is obvious variability, probably associated with flickering, as well as a possible sinusoidal modulation, but no eclipses.
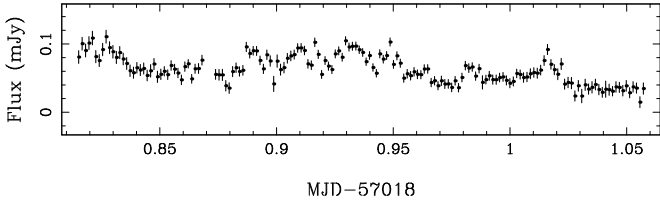
Figure B3. ASASSN-14gl light curve observed during quiescence on 2014-12-27 with *pt5m*.
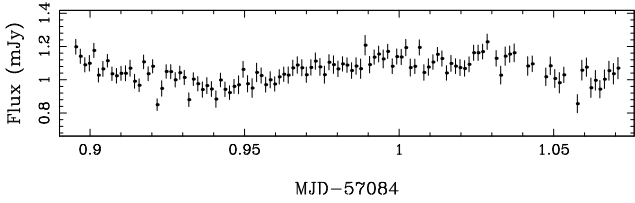
Figure B4. ASASSN-14gu light curve observed on 2015-03-03 with *pt5m*. The periodic modulation is present in outburst and in quiescence, meaning that it cannot be attributed to superhumps.
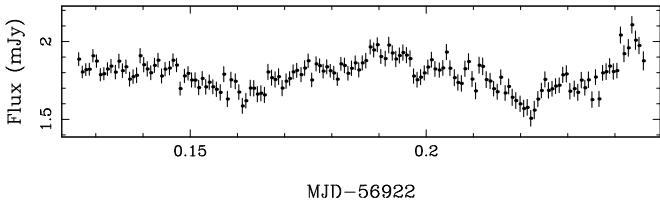
Figure B5. ASASSN-14hk light curve showing superhumps, observed during super-outburst on 2014-09-21 with *pt5m*.
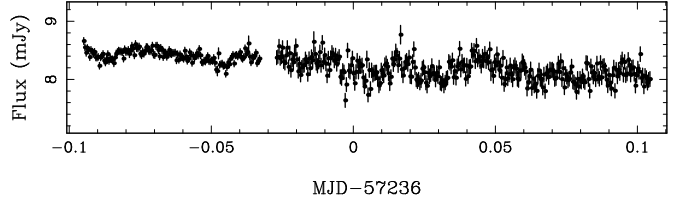
Figure B6. ASASSN-15ni light curve observed on 2015-08-01 during the decline from outburst with *pt5m*. The gap in the light curve is due to the telescope conducting a pier-flip as the target transited the observers meridian. After the pier-flip, a different (fainter) comparison star had to be used. This explains the difference in the size of the error bars before and after the gap.
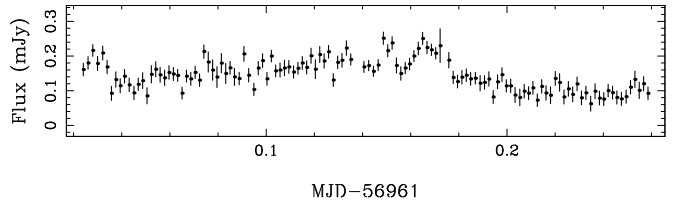
Figure B7. CSS090219:044027+023301 light curve observed during quiescence on 2014-10-30 with *pt5m*.
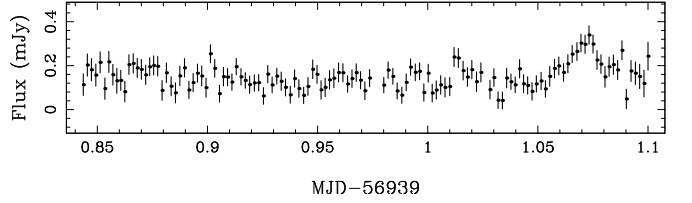
Figure B8. CSS091116:232551-014024 light curve observed during quiescence on 2014-10-09 with *pt5m*.
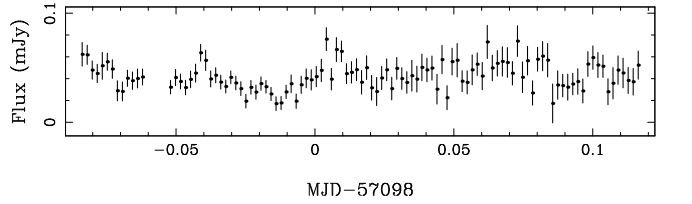
Figure B9. CSS100508:085604+322109 light curve observed in quiescence on 2015-03-16 with *pt5m* in windy conditions. The sporadic variability is attributed to flickering.
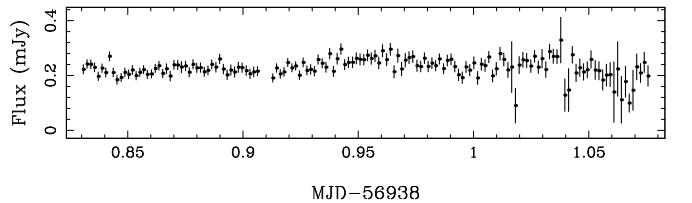
Figure B10. CSS100520:214426+222024 light curve observed during quiescence on 2014-10-08 with *pt5m*. The disruption towards the end is due to patchy cloud cover.
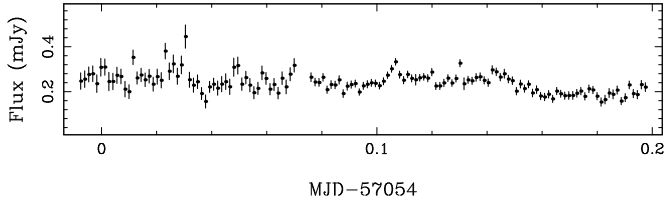
Figure B11. CSS110114:091246-034916 light curve observed during quiescence on 2015-01-31 with *pt5m*.
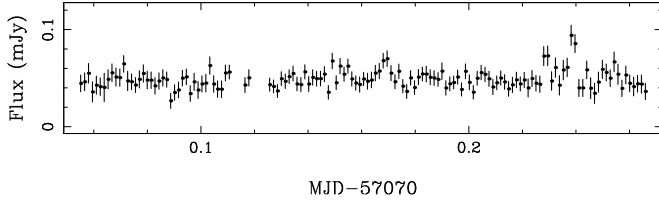
Figure B12. CSS110226:112510+231036 light curve observed during quiescence on 2015-02-16 with *pt5m*.
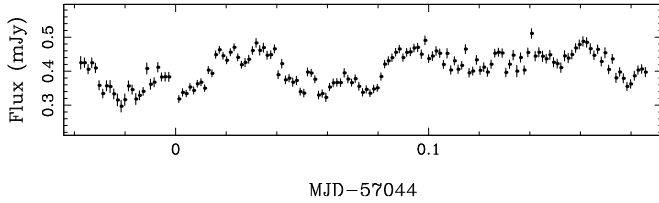

Figure B13. CSS130906:064726+491542 light curve observed during quiescence on 2015-01-21 with *pt5m*. Variability could be attributed to flickering, or movement through hot pixels on the CCD detector (see text for details).
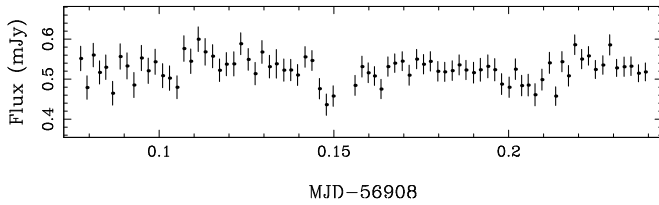

Figure B14. CSS140901:013309+133234 light curve observed on 2014-09-07 with *pt5m*. Here the system is fading from outburst but some superhump signals are still present.
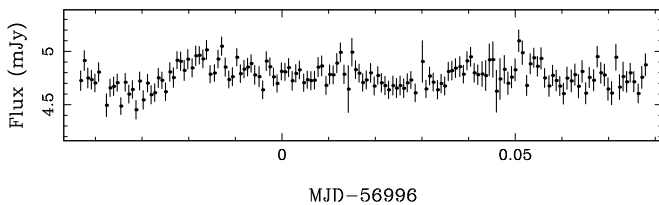
Figure B15. CSS141005:023428-045431 light curve observed whilst fading from outburst on 2014-12-04 with *pt5m*. This light curve is one of several observations on different nights that display periodic features resembling superhumps, although stochastic flickering is not ruled out as the cause for this variability.
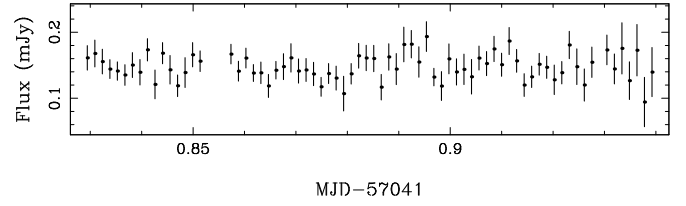
Figure B16. CSS141117:030930+263804 light curve observed in quiescence on 2015-01-19 with *pt5m*. Some thin overhead cirrus affects the quality of the light curve.
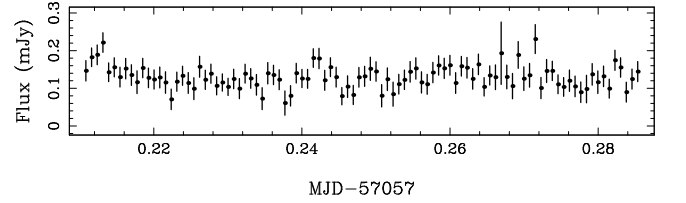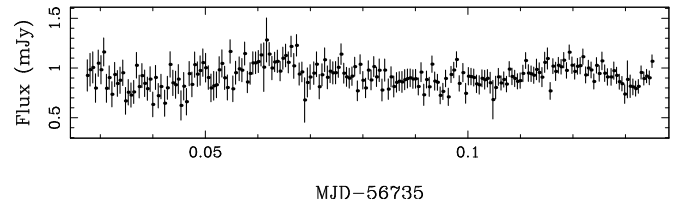

Figure B17. Gaia15aan/ASASSN-14mo light curve observed during the decline from outburst, on 2015-02-03 with *pt5m*.
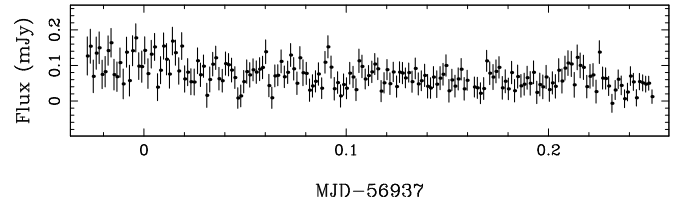

Figure B18. MASTER OT J034045.31+471632.2 light curve observed during quiescence on 2014-10-06 with *pt5m*.
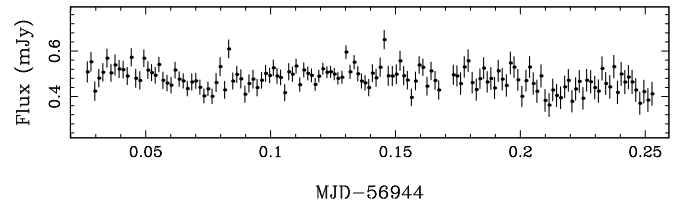

Figure B19. MASTER OT J041923.57+653004.3 light curve observed on 2014-09-21 with *pt5m*. The variability may be periodic, or attributed to flickering.
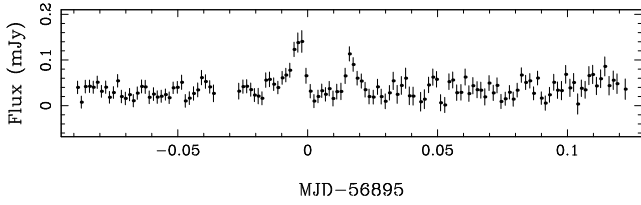

Figure B20. MASTER OT J171921.40+640309.8 light curve showing superhump-like variability, observed during outburst on 2014-03-18 with *pt5m*.
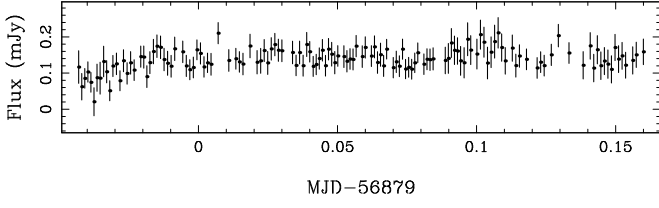
Figure B21. MASTER OT J194955.17+455349.6 light curve observed in quiescence on 2014-08-09 with *pt5m*.
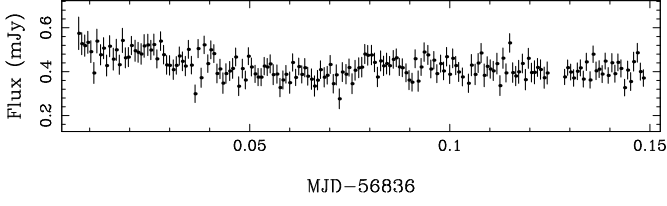

Figure B22. MASTER OT J201121.95+565531.1 light curve observed during the decline from outburst on 2014-06-27 with *pt5m*.

Figure B23. MASTER OT J202157.69+212919.4 light curve observed on 2014-08-25 with *pt5m*. The two peaks in the centre are caused by the apertures tracing across hot pixels on the CCD.
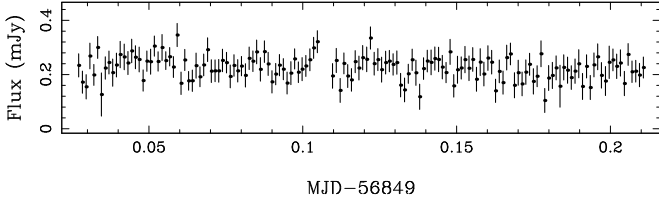
Figure B24. MASTER OT J203421.90+120656.9 light curve observed during outburst on 2014-07-10 with *pt5m*.
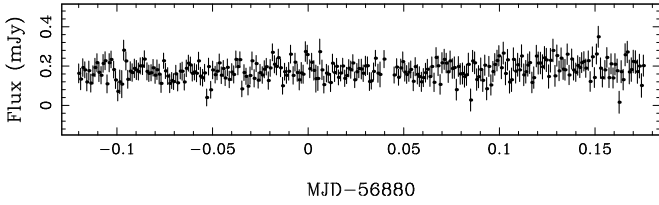
Figure B25. MASTER OT J210316.39+314913.6 light curve observed during quiescence on 2014-08-10 with *pt5m*.